

Politecnico Di Torino

Degree course in Mechatronics Engineering



Master of Science Thesis

Radial force in elastomeric seals for pneumatic cylinders (measurements
and analysis)

Author:

Soroush Pourhashemi Dehkordi

Supervisors:

Luigi Mazza

Carmen Visconte

Abstract

This study deals with the experimental evaluation of contact pressure at the interface between an elastomeric rod seal for pneumatic cylinders and its metallic counterpart without interposing any intrusive measuring device. A modification of test bench, which is able to measure the radial force exerted by a rod seal displaced at constant velocity on a sensorized portion of a cylinder rod over time, was designed and manufactured. The seal was pressurized to reproduce actual working conditions. A data post processing methodology was developed for an indirect evaluation of contact pressure starting from the experimental data set of the radial force exerted by the seal on the rod. At first, the measured radial force signal was filtered by the specific filter; then, contact pressure distribution was computed as a function of radial force time derivative, seal velocity and rod diameter. Preliminary experimental results are presented in three different test condition.

Dedication

I wish to thank all those who helped me to complete this goal to them my gratitude goes. It was a period of intense learning, not only in the technical field but also on a personal level. I would like to thank my relatives, in particular my parents and my sister and my brother, for the support and love received in these years. To my friends and colleagues who in one way or another have shared their precious support, morally and physically, thank you for accompanying me on this journey. Special thanks goes to Professor Luigi Mazza and Professor Carmen Visconte. I dedicate this goal to the memory of my grandparents, for their unconditional love, for kindness, patience and life lessons.

Table of Contents

Abstract.....	ii
Dedication.....	iii
List of Tables	v
List of Figures.....	vi
Chapter 1 Introduction	9
Chapter 2 Literature review	10
2.1 Photoelastic Reflection Technique	11
2.2 Tri-dimensional eccentricity model of a rod lip seal	12
2.3 Employed Film Sensors	18
3.1 Test Bench	27
3.2 Modification of Test Bench	30
3.3 The Parts of Test Bench.....	39
Chapter 4 Measurement	47
4.1 Indirect measurement of contact pressure.....	47
4.2 Calibration of the Load Cell	48
Chapter 5 Experimental study.....	53
1-5 Experimental Procedure	53
2.5 Starting the Test	54
2.5 Recording data	57
3.5 MATLAB.....	59
4.5 Analyzing Test Results	77
Conclusion	78
References.....	80

List of Tables

Table 4.1 Load cell data.....	52
Table 4.2 Load cell data.....	53
Table 5.1 Test Conditions.....	56
Table 5.2 Test Conditions.....	56
Table 5.2 Test Conditions.....	57

List of Figures

Figure 2.2 Principal dimensions of the seal groove (in mm).	14
Figure 2.3 Reaction force as a function of the applied misalignment.	14
Figure 2.4 Proposed process scheme.	17
Figure 2.5 Comparison between experimental, numerical and analytical results.....	18
Figure 2.6 Schematic of the lip seal.....	19
Figure 2.7 Temperature profile of the seal mated with 25.4 mm shaft and the Coefficient of friction was taken as 0.12	22
Figure 2.8 Schematic representation of the calibration test rig.	24
Figure 2.9 Colour intensity distribution on the film sensor sheet.	25
Figure 3.1 a) Sensorized portion of the rod (the full contact area between the seal and the sensorized rod is in grey); b) axisymmetric contact pressure distribution; c) elementary portion of contact area.	28
Figure 3.2 Sketch a) and photo b) of the measuring portion of the test bench.	29
Figure 3.3 sliding bearing	30
Figure 3.3.1 drawing sliding bearing	31
Figure 3.4 Pneumostatic cylinder	32
Figure 3.4.1 Pneumostatic cylinder	32
Figure 3.4.2 Drawing of Pneumostatic cylinder	33
Figure 3.5 Seal holder	34
Figure 3.5.1 Seal holder	35

Figure 3.5.2 Drawing Seal holder	35
Figure 3.5.3 Drawing Seal holder	36
Figure 3.5.3 Assembly of parts	37
Figure 3.5.3 Test Bench	38
Figure 3.6 Electrical Connection	39
Figure 3.7 Load cell	40
Figure 3.8 Acquisition system	41
Figure 3.9 Speed Sensor	42
Figure 3.10 pneumatic valves	43
Figure 3.11 Electrical controller of pneumatic valve.....	44
Figure 3.12 Air supplier for seals	45
Figure 3.13 Manometer.....	46
Figure 4.1 Dynamic measurement of the seal/rod radial force.	48
Figure 4.2 calibration setup.....	49
Figure 4.3 calibration setup.....	49
Figure 4.4 Calibration Test	52
Figure 5.1 Experimental Procedure	53
Figure 5.2 Complete Test Bench	56
Figure 5.3 Software area	57
Figure 5.4 Test Procedure	58
Figure 5.5 Matlab Command	60
Figure 5.6 Force Plot.....	61
Figure 5.7 Three test figure together before synchronizing.....	62

Figure 5.8 Three for loops for finding the starting points	63
Figure 5.9 Matlab command	64
Figure 5.10 Matlab command	65
Figure 5.11 Three force at the same starting points	65
Figure 5.12 Total model in Simulink	67
Figure 5.13 Filter design and frequency response	67
Figure 5.14 Chebysev Filter frequency response	68
Figure 5.15 Original Signal compared to Filtered signal	69
Figure 5.16 Simulink	70
Figure 5.17 Hole Simulink model	71
Figure 5.18 Contact Pressure versus displacement	72
Figure 5.19 Contact Pressure versus Displacements	73
Figure 5.20 Contact Pressures at same velocity with different pressure	74
Figure 5.21 Contact Pressures at Different velocity	75
Figure 5.22 Contact Pressure in different frequency	76

Chapter 1

Introduction

The necessity of analyzing elastomeric seals is neither for choosing best dimension nor ability to use different type of material, Is just due to the consideration of some great operating parameters such as applied loads, working pressure, lubrication conditions, temperature and sliding velocity. Indeed, the studies of the contact characteristics at the rubber-metal interface help us to understand which not only the seal capability is depend on contact pressure but also strength of the frictional force. According to the forceful studies that have been done numerically and experimentally on the road seal for achieving these operating parameters, Specific test bench in order to measuring the contact pressure at the seal-road has been designed and manufactured according to the solution of Ref [1].An specific seal holder which would play as an appropriate seat role for the road seal and permits to pressurize the sealing lip of the seal, Specific Pneumostatic bearing used to obtain smooth motion even at low velocity, Also a couple of load seal for obtaining final voltage after applying force on the seal.

Finally, we have done appropriate modification on some parts of test bench. In particular, it is possible to identify: the seal holder (Figure 3.5) which permits us to pressurize the seal as much as close to the sealing leap, the pneumatic cylinder (Figure 3.4) which provide a proper smooth and accurate motion of cylindrical road that obtained and guaranteed by adding a couple of sliding bearings (Figure 3.3) inside the pneumatic cylinder.

Chapter 2

Literature review

Many researches with the different kind of approaches have been done around the characteristics of contact interface between lip seal and its counterpart. Some of them are introduced in the following.

Photoelastic reflection technique, Numerical evaluation of contact pressure, Employing film sensors, Employing sensor for the static measurement ,Non-intrusive ultrasonic method ,Contact pressure of PTFE road seal and finally Developing an specific test bench.

2.1 Photoelastic Reflection Technique

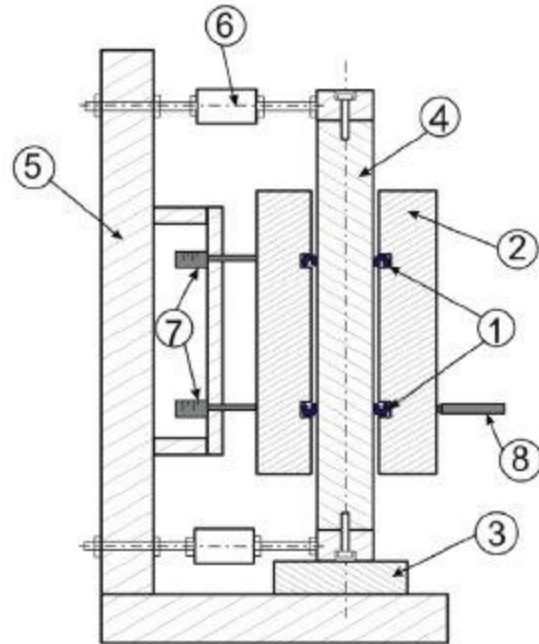
Bignardi[1] processed experimental data obtained on a pneumatic lip seal by a photoelastic reflection technique to compute analytically the contact pressure distribution at the seal rod interface, By more detail the contacting surface between the lip seal and the rod was investigated by means of a specific experimental procedure employing pressure sensitive film. Measurements performed on a rectilinear seal. To this aim, a segment cut from a high diameter ring (500mm diameter) for testing it as straight specimen. A Fuji pre-scale pressure sensitive film placed between the lip surface and the faced plate has performed tests. The film is made up of two matched paper film is coated with a color developing material. Applying a load on the film microcapsule are broken so that a distribution of magenta color with a certain density obtained depending by true pressure and magnitude. As there is, a pressure below which no capsule will be broken this sensor has minimum threshold below which stress values could not registered. In addition, there is pressure, which will break all the capsules corresponding to an upper threshold. Although a pre-calibrated densitometer which converts magenta tones into pressure values could be supplied by the manufacturer an own calibration procedure was developed using a suitable test rig. It has to be note that complex temperature humidity charts, needed for proper calibration curve selection for densitometer use, are not required since both calibration tests and final measurements on the lip seal are obtained under identical environmental conditions.

2.2 Tri-dimensional eccentricity model of a rod lip seal

Piendó,[2] built an analytically Tri-dimensional eccentricity model of a rod lip seal extrapolating contact pressure distribution from finite elements simulations and experimental measurements. A suitable test rig was designed and assembled to measure the resultant contact forces on seals when the rod is radially displaced (Fig.2.1). Seals under test (1) are mounted in the test chamber (2), one on each cylinder end. The rod rests on a low friction and high stiffness polymeric base (3). The cylinder rod (4) is vertically positioned in order to minimize the weight effects and it is fixed to the frame (5) through a couple of tension/compression load cell with an accuracy of ± 0.01 N (6). Misalignments are applied by means of two micrometric positioners (7) fixed to the frame. Cylinder position is controlled by means of a vertically guided which has a resolution of $1 \mu\text{m}$.

Measurements were carried out on commercial rod lip seal, made of TPU (thermoplastic polyurethane), suitable for a 45 mm diameter rod (Fig. 2). Misalignment were performed at room temperature and in the absence of supply pressure. Before seal installation, a small amount of oil (0.1 ml) was applied on the contact surfaces. The cylinder bore was displaced in radial direction only. Measurements were carried out under the controlled environment, $20 \pm 1^\circ \text{C}$.

a



b

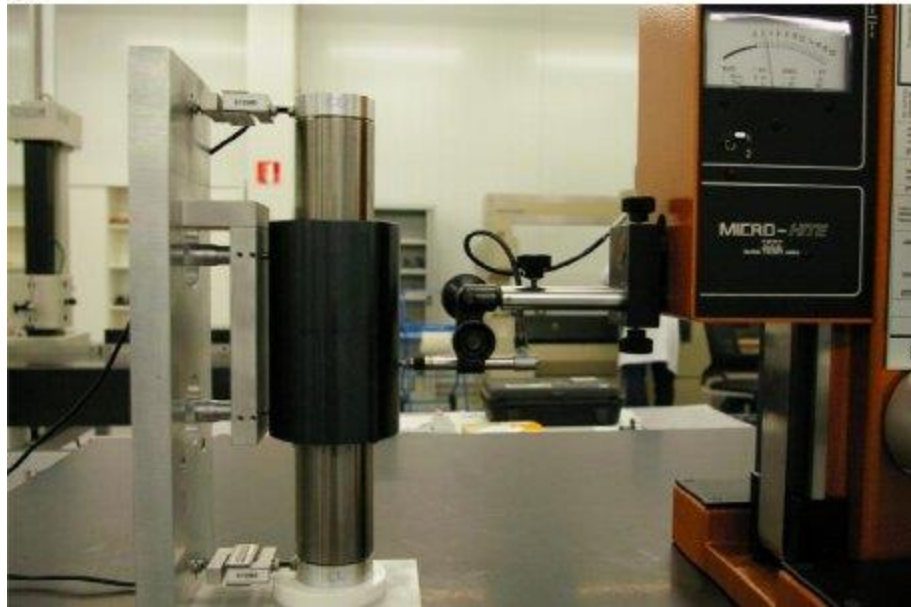


Figure 2.1 Experimental setup for misalignment tests (a) schematic view and (b) test rig assembly

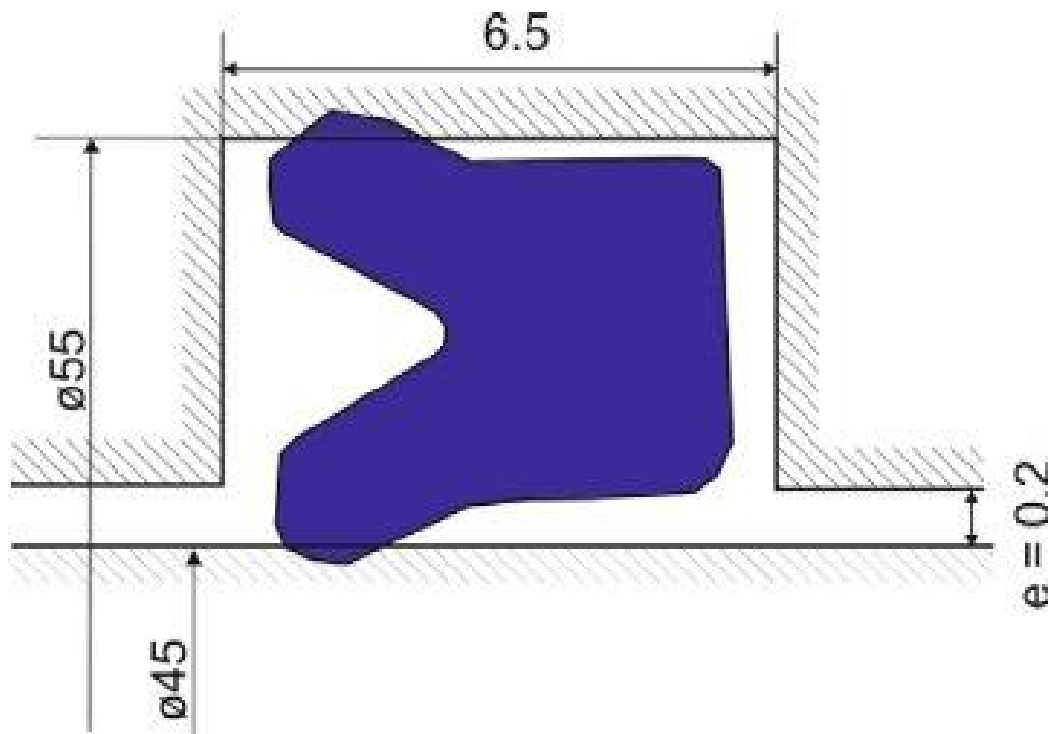


Figure 2.2 Principal dimensions of the seal groove (in mm).

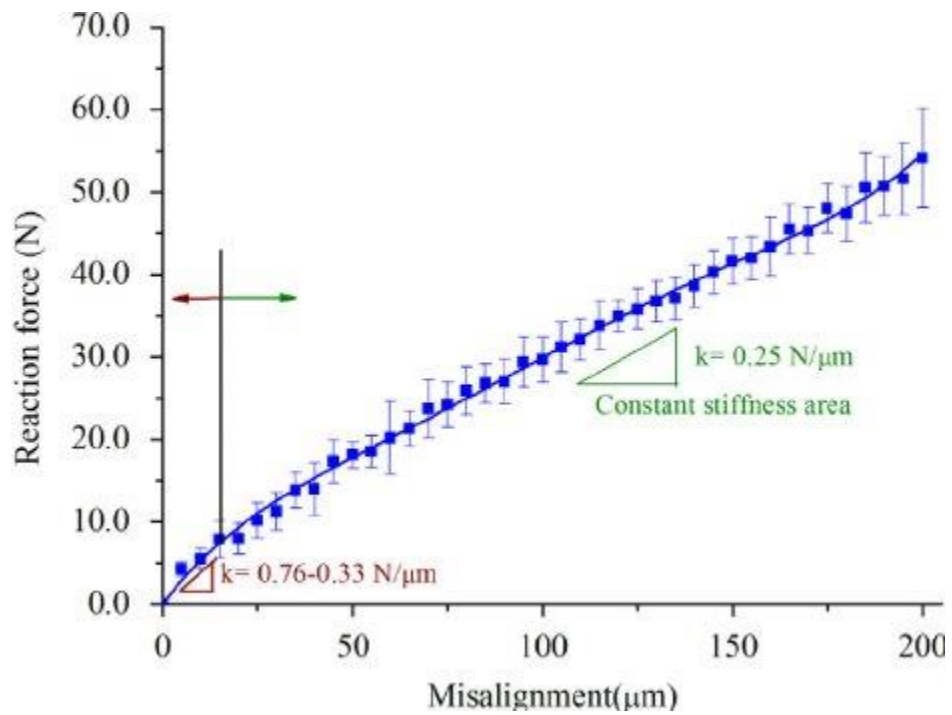


Figure 2.3 Reaction force as a function of the applied misalignment.

At the beginning of the process, the cylinder rod was vertically placed adjusting the micro-positioners. Subsequently, consecutive known radial misalignment values were applied. The maximum applicable misalignment is limited by the nominal gap, e , with a value of 0.2 mm (Fig.2.5). Misalignment were applied in step of $5\mu\text{m}$ up to the maximum allowed one. Reaction forces at each step are measured by means of the load cell after verifying and adjusting the vertical alignment of the cylinder. Measurements were applied 3 times. (Fig.2.5) shows the reaction force curves of a set of consecutive tests relative to the misalignment applied to the bore. Results showed a good repeatability. As can be observed, the stiffness of the whole seal in the misalignment direction is not constant. In particular, the seal presents the stiffest response when the rod misalignment is about five μm ($\text{KE}0.76 \text{ N}/\mu\text{m}$). Above that eccentricity value, the stiffness decreases exponentially until reaching a nearly constant value for rod misalignments $Z5 \text{ mm}$ ($\text{KE}0.25 \text{ N}/\mu\text{m}$). Between a seal and the mounting rod, as a function of rod misalignment. The proposed analytical model has been completed and adjusted by means of numerical results. To this end, first of all, a plane model and a tri-dimensional model of the selected seal (Fig.2.7) were developed and numerical simulations were carried out. Then, a geometrical interference model and contact equations were formulated. It is particularly relevant to highlight that even if a quasi-static Case is being studied; contact equations are based on the kinematic Coulomb model. Hence, this assumption involves a simplification of the problem that could be valid due to the nature of the tests, where an increasing load is monotonically applied to the rod. Moreover, the simplified model may be acceptable since the main goal of this work is to avoid time and expensive computational costs of a 3D numerical simulation. The analytical

Model was validated by means of the experimental results presented in the previous section. (Fig.2.4) shows the flow chart of the modelling procedure. A numerical study was performed to complete the analytical model described in detail in the next section. Both, a plane model and a tri-dimensional model of the rod lip seal were developed in an Ansys Workbench environment. Seal geometry was obtained by means of an optical microscope (Leitz, model Libra 200). The plane strain model was built in order to obtain the functional contact relation between the rod and the seal, as a function of the seal section compression. Normal and tangential forces taken from simulations on the plane model are mandatory inputs to build the analytical model. Two tri-dimensional models were developed in order to validate the analytical model results step by step: an ideal frictionless one, and another one which considers frictional contacts. Both numerical models were built by means of quadrilateral and triangular elements. Due to the symmetry of the geometry and boundary conditions, only a half of the seal was modelled in the case of the tri-dimensional model. Moreover, this simplification allows reducing the computational cost of each simulation. The bi-dimensional model was composed of 1609 elements and the tri-dimensional one of 33,586 elements. The mesh used is the result of a number of analyses performed in order to determine the element sizes that do not produce significant variation in calculation precision.

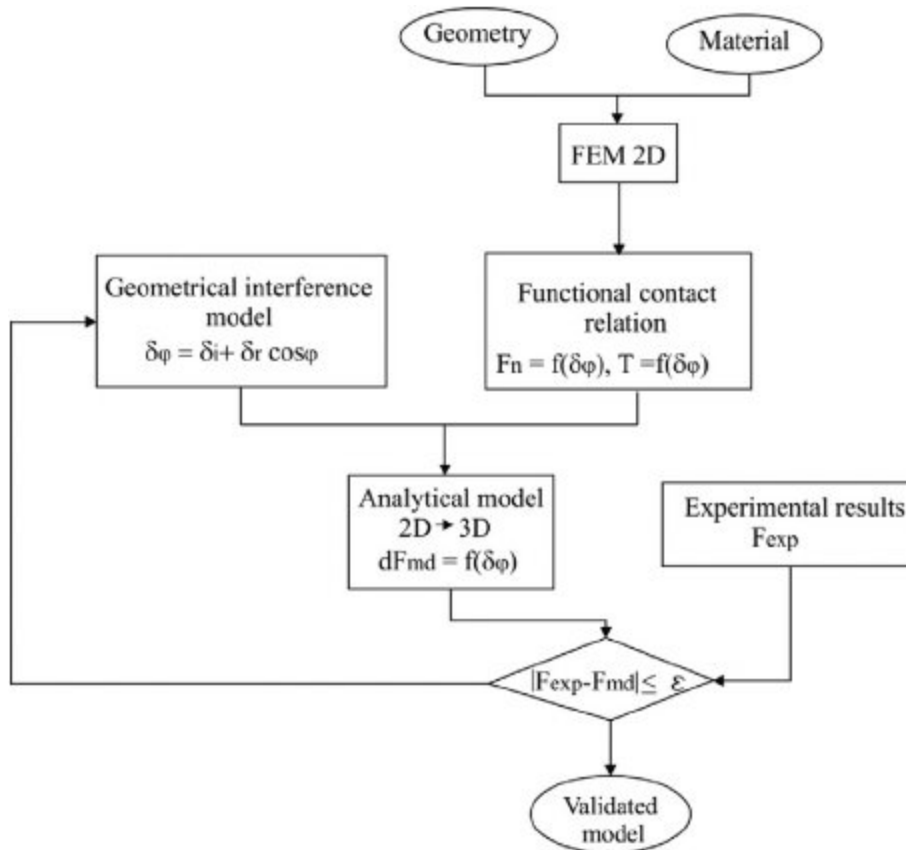


Figure 2.4 Proposed process scheme.

Experimental results were used in order to validate the analytical model proposed in this work. It was found a good correlation between experimental and the analytical results of the model that includes tangential and frictional effects, i.e. frictional contacts, should be assumed. (Fig. 2.5) shows a comparison between experimental, numerical and analytical results, (D), and it presents the error between analytical and experimental results in absolute terms. The maximum difference between the analytical an experimental result in absolute terms is approximately 6.4 N, which occurs for the highest misalignment.

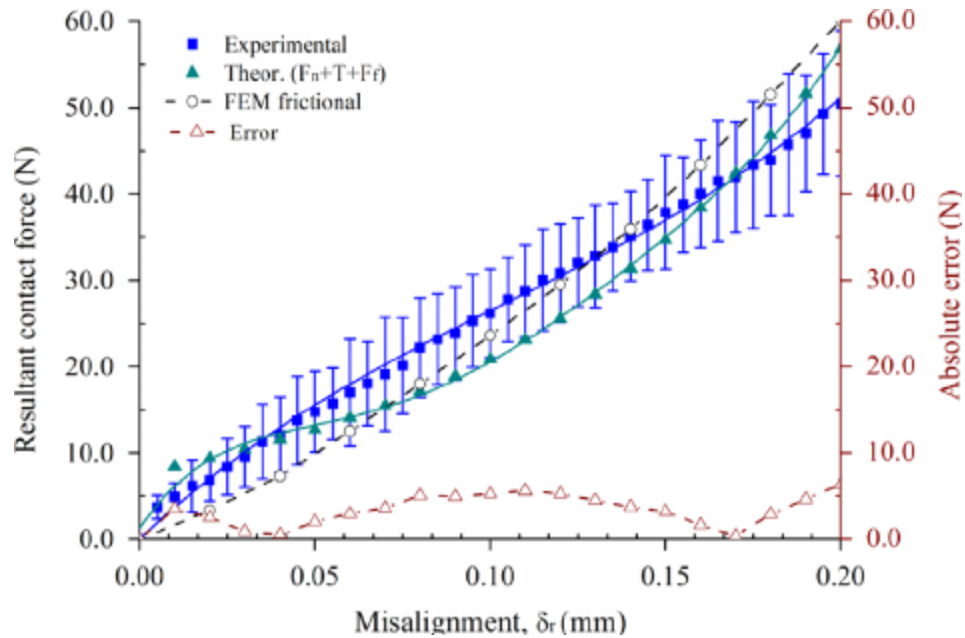


Figure 2.5 Comparison between experimental, numerical and analytical results.

2.3 Employed Film Sensors

Lee et al [3]. Shaft seal is a critical component for rotating machinery. It allows for the relative motion between the shaft and the support housing and seals the lubricant from leaking into outer compartment. Among the seals, the lip seal is one of the commonly used. The design in the dimensions and geometry has crucial influence on the performance of the lip. The sealing capability and life of the seal are directly related to the contact characteristics at the lip. The contact width and the pressure profile in the contact region between the lip and shaft are two major performance indices of the lip seals. (Fig.2.6) shows the schematic of an installed lip seal and its components.

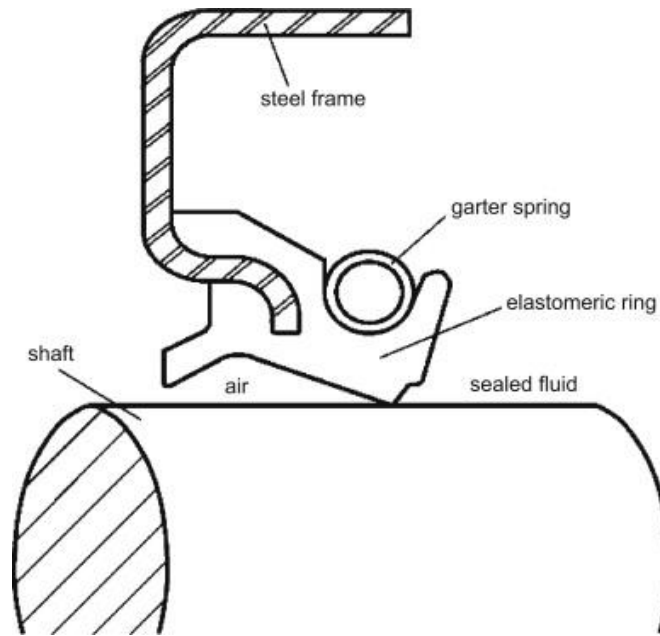


Figure 2.6 Schematic of the lip seal.

Although the former studies had employed the FEA in the simulation of the lip seal, the use of the FEA tool in the investigation of the pressure profile and contact width of the rotating lip seal was rarely found. In addition, a novel experimental set up presented in this study was able to measure the contact width and the pressure profile of the lip seal under different magnitudes of diametric interference between the seal and shaft. This design provides the designer a viable tool to evaluate the contact behavior for the seal at various diametric interferences easily. The FEA software MARC was employed in the numerical simulation of this study. The rubber for this lip seal was assumed to be a Mooney–Rivlin material [7] with the following constants: $C_{10} = 0.84$ MPa, $C_{01} = 0.38$ MPa. These constants were curve-fitted from the experiment conducted on the unit-axial tensile testing. The cross-section of the selected lip seal is shown in Fig.1. Because the lip seal is axisymmetric in nature and the steel frame is much more rigid than the rubber, only axisymmetric element on the rubber portion was meshed. The boundary of the rubber

adhered to the steel frame was assumed fixed in displacement. The surface of the lip seal on the side of the lubricant compartment was subjected to the fluid pressure of the lubricant. The other side was taken as the atmospheric pressure. To increase the radial force required to provide sealing function for the ordinary seals, there is a pre-tensioned garter spring on the lubricant side of the lip. In this study, the cross-section of the garter spring was assumed to be rigid cylinder. The spring force exerted by the garter spring was simulated by a linear spring connected between the axial center of the seal and the center of the cylinder. The spring constant of the linear spring was 2.9 N/mm and the pre-tension force was 12.9 N [8]. In this study, the temperature distribution due to the heat generation of friction work was also simulated. The following material constants on the thermal behavior the rubber were used: coefficient of heat conduction 0.43 W/m K; coefficient of thermal expansion $9.44 \times 10^{-5}/K$. The ambient temperatures of the lubricant and atmosphere were assumed 40 and 20 °C, respectively. Moreover, the coefficients of heat convection for the lubricant side and air side were 200 and 10 W/m K, respectively [6]. In the simulation, there were two contact regions: one was the lip and the shaft, the other was the garter spring and its rubber seat. During the analysis, the shaft was assumed to be rigid and moved upward in different amounts to simulate the shaft and lip seal in different amounts of diametric interferences. In the simulation, there were two contact regions: one was the lip and the shaft, the other was the garter spring and its rubber seat. During the analysis, the shaft was assumed to be rigid and moved upward in different amounts to simulate the shaft and lip seal in different amounts of diametric interferences. (Fig.2.7) presents the schematic diagram of the experimental set up in measuring the contact width and the pressure of lip seal. The inflatable mandrel was employed to simulate the shaft with different diameters. The

mandrel was fabricated using rubber tube with one end sealed by plug and the other connected to pressure source. The tube was surrounded by a metallic spiral stripe to provide the surface bending rigidity for contact loading. The spiral was able to conform to the dilation of the inner inflatable tube and still remained in circular cross-section. By adjusting the pressure inside the inflatable tube, the outer diameter of the mandrel could be changed accordingly. The change in the diameter of the mandrel was measured by the extensometer composed of two cantilever arms. The deflection at the tip of the cantilever arm was measured via the strain gauge mounted on the arm with calibration. The lip seal was fixed on the specimen platform with the mandrel inserted through its bore. The string attached to the top of the mandrel provided the support of the mandrel before it is inflated. Because the top of the mandrel was free to move laterally, it should align concentrically and automatically with the bore of seal. This could eliminate the problem in alignment. The pressure at the contact zone of the lip acts on the rotating shaft during normal operation of the lip seal. This normal loading plus the relative sliding between the lip and shaft surface induces the friction. Consequently, the frictional work is dissipated into heat generation. The power of this heat generation can be calculated by multiplying the friction force with the linear speed on the surface of the shaft. In this study, the nodal contact force was used in the calculation of the heat source at nodal point within the contact zone. The generated heat was conducted away from the contact zone through both the rubber seal and the steel shaft. Usually, the metal shaft has higher coefficient of heat conduction. Therefore, more heat would be dissipated through the shaft than the seal. However, for more conservative design, half of the generated heat power was assumed to be dissipated via the seal. In

addition, the rotational speed of the shaft was chosen as 600 rpm. The other speed can be used without any difficulty.

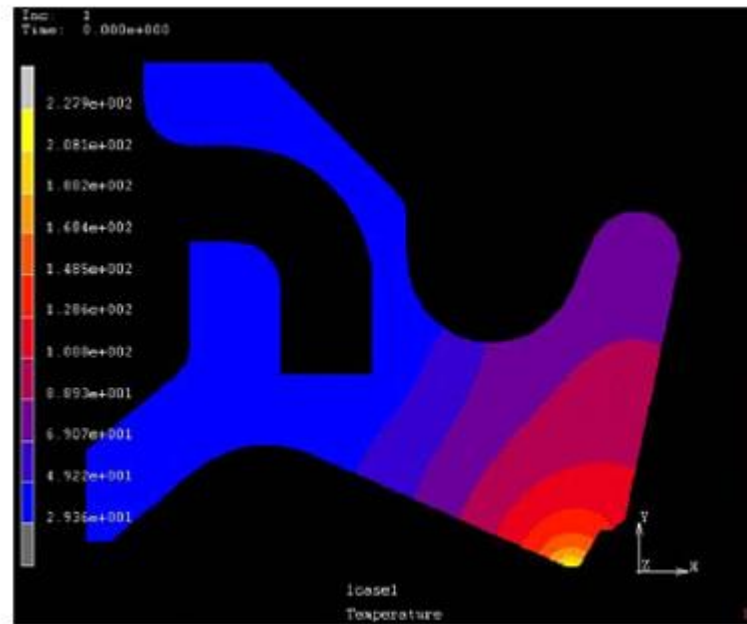


Figure 2.7 Temperature profile of the seal mated with 25.4 mm shaft and the Coefficient of friction was taken as 0.12

(Fig. 2.7) shows the steady temperature contour of the seal mated with the 25.4 mm shaft and with the 0.12 coefficient of friction. It could be expected that the temperature decreased as the distance from the contact zone increased. The maximum temperature at the contact zone can be used to compare with the tolerance temperature specified for the rubber material. If the temperature was higher than the allowable working temperature, the design should be modified to have required life span of the seal.

Belforte et al [4]. Aim of this paper is to present a general experimental methodology for measuring contact pressure on pneumatic elastomeric seals by means of film sensors. A first set of experimental tests was carried out on a lip seal rectilinear specimen, for a relatively easy and rapid evaluation of the experimental method effectiveness and reliability. Then, the experimental procedure was applied on two different commercial pneumatic piston seals, mounted on a suitably modified actuator. In order to evaluate results repeatability, an extensive experimentation was carried out, applying different pressure loads, in dry and lubricated conditions. Finite-element models of the seals, reproducing actual operating conditions and taking into account material nonlinearities, were developed. Experimental and numerical results were compared in various operating conditions. In order to investigate the contacting surface between a pneumatic seal and its counter face, pressure-sensitive films were employed. This kind of sensor is made up of two-matched paper like layers: a first layer is coated with a microencapsulated colour forming material; a second layer is coated with a colour developing material. The sensor thickness is very low (about 0.2 mm). Applying a load, microcapsules are broken, releasing a liquid that passes onto the active layer and reacts with it; as a result, a distribution of magenta color, with a certain density, is obtained, depending by true pressure distribution and magnitude. As there is a pressure below which no capsule will be broken, this sensor has a minimum threshold below which stress values cannot be registered. Also, there is a pressure above which all capsules are broken, corresponding to a saturation threshold. A limitation of this kind of sensor is that it is a single-recording instrument, which cannot be used to study transient phenomena. The manufacturer provides calibration charts and colour samples, which can be used to convert optical-density readings into pressure. Using

this approach, a limited pressure resolution can be obtained, since only few colour samples are provided. Therefore, an own calibration procedure was developed, using the test rig shown in (Fig.2.8) The sensitive film (1) is placed on a smooth surface (2) and faced to chamber (3), which can be gradually pressurized. Loading film sensors by air pressure, rather than by calibrated weights, was preferred, in order to obtain a better uniformity of load distribution from the film edges.

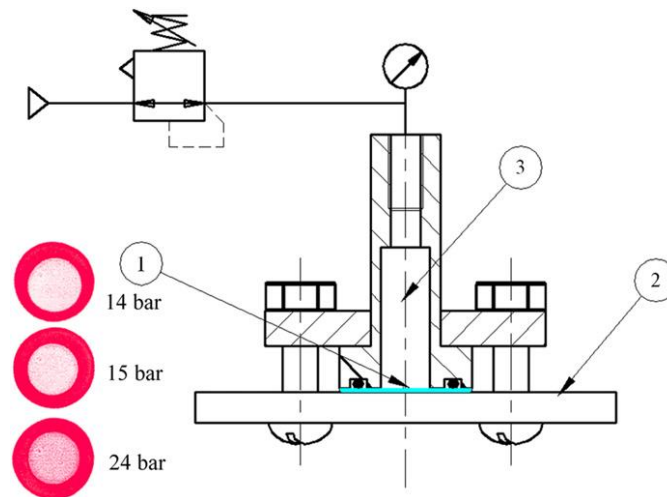


Figure2.8 Schematic representation of the calibration test rig.

The calibration curves needed to evaluate imprints from experimental tests on seals were so obtained. Measurements highlighted that the film sensors operation is almost linear inside the measuring range and is sensitive to humidity only at fairly High values. In fact, although varying humidity from 25% to 50% had hardly any effect, varying this parameter from 50% to 75% produced an increment of about 40% in colour intensity and a higher pressure sensitivity [7]. Experimental tests were analysed using image-processing techniques. Having digitalised imprint images, a three-dimensional matrix is obtained (see

Fig.2.9) gathering information on pixels coordinates over the contact surface and on the corresponding colour intensity values. An average value of colour intensities can be, therefore, computed along the contact length L

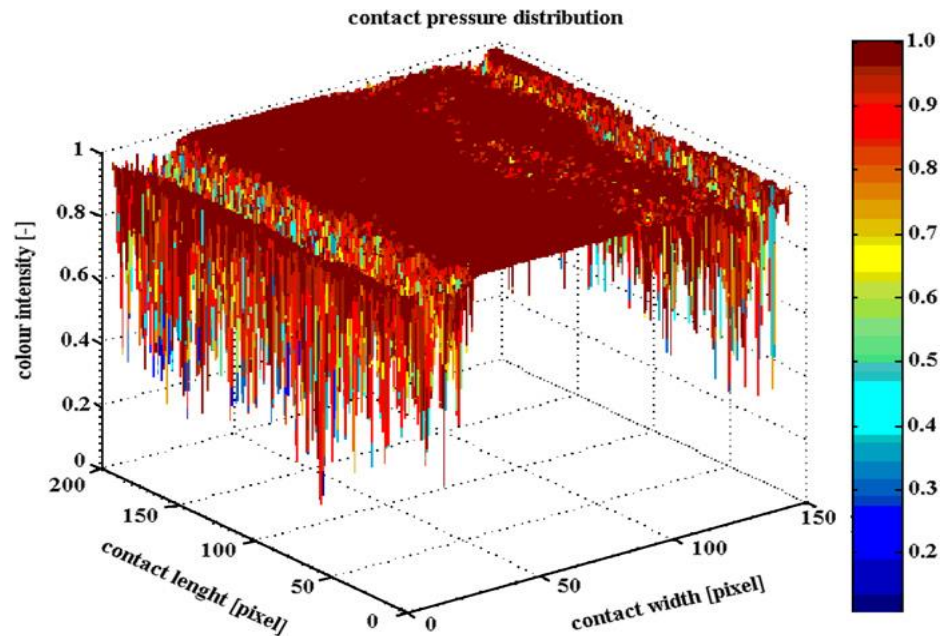


Figure2.9 Colour intensity distribution on the film sensor sheet.

A numerical study was performed, using a finite-element analysis commercial software, on the same seal specimens that were experimentally tested. Simulations were performed on a plane model of the rectilinear specimen described in Section 2.2 and on axis-symmetric models of the two seals described in Section 2.3, using eight-node plane elements (two degrees of freedom at each node, translation in the nodal x and y directions). A surface-to-surface contact formulation was chosen to simulate contact with the seal seat and with the

surface of the plate, in the case of a rectilinear specimen, or of the cylinder bore, in the case of whole seals; the plate/bore surface and the seat were considered as rigid elements. Boundary conditions took into account friction at the seal contact surfaces using the Coulomb friction model. The friction coefficient values are $f=0.4$ on the seal-seat contact; $f=0.4$ or $f=0.05$ between the seal and the plate/bore surface, respectively, in case of dry or grease-lubricated contact. The seal material (NBR elastomer, with hardness of about 75 IRHD) was modelled considering an incompressible, isotropic, hyperelastic material, well represented by the Mooney–Rivlin formulation. In particular, a five constants Mooney–Rivlin formulation was employed for the rectilinear specimen; these constants were computed by the numerical code fitting experimental data obtained. A two constants Mooney–Rivlin formulation was employed for modelling the piston ring seals. Poisson's ratio ν was assumed to be equal to 0.4995. Load was applied step by step, reproducing actual working conditions; in particular, at first, mounting was simulated, according to nominal dimensions; subsequently, a pressure load was applied, set to 0.2, 0.4, 0.6 MPa.

Tests on the rectilinear specimen were initially carried out, for a relatively easy and rapid evaluation of the experimental method effectiveness and reliability. These preliminary tests highlighted that a careful manipulation and positioning of the film sensors is needed in order to avoid inconsistent results. For this reason, each test, on the same sample and under the same load condition, was repeated at least six times, in order to identify and cut-off eventually dispersed data

3.1 Test Bench

A test bench for the indirect measurement of contact pressure at the seal-rod interface was designed and manufactured.

A sketch of the measuring portion and a photo of the manufactured test bench are shown in (Fig. 3.1 a) and b), respectively. In particular, it is possible to identify: the seal holder (1), which permits to pressurize the sealing lip of the seal; a Pneumostatic bearing (2), used to obtain a smooth motion even at low velocity; the fixed parts (3) and (30) of the measuring rod and the Sensorized rod portion (4); the couple of load cells (5), which measure the radial force signal over time; precision screws (6), which were used to adjust the gap h_1 between the two portions of the rod correctly (see the detail in Fig. 3a); the pair of pneumatic bearings (7) and the pneumatic pad (8), which permit to correctly align and center the Sensorized rod portion (4) with respect to the rod extension (30). In particular, the pair of pneumatic bearings (7) has also the aim to balance the friction force exerted in z-direction and any torque produced about the x or the z axis; the pneumatic pad (8) balances any torque about the y axis. The choice of pneumatic guide bearings, namely low friction bearings, ensures that the seal radial force F exerted in y-direction is correctly measured by the load cells; any additional friction would misrepresent the measurement. More details on the test bench characteristics can be found in Ref. [5]. In this test bench, the generation of the measuring signal is obtained by displacing the sensorized portion of the rod in the negative y-direction. Since this displacement causes a modification of the

shape and of the diameter of the rod, it has to minimize. To this aim, load cells FGP FN 3030 (accuracy $\pm 0.1\%$ F.S) with a full scale of 1000 N, definitely higher than that required, were chosen to ensure a high stiffness; thanks to the parallel assembling configuration, the equivalent stiffness of the measuring device is of $4.2 \cdot 10^7$ N/m. Both the load cells were calibrated out of the test bench. After having mounted them in the working configuration, a known weight was hanged on the Sensorized portion of the rod, to further verify that the sum of the force measured by each cell was equal to the loading weight. The radial force signal was recorded by a NI USB-6229 data acquisition system at a frequency of 1 kHz.

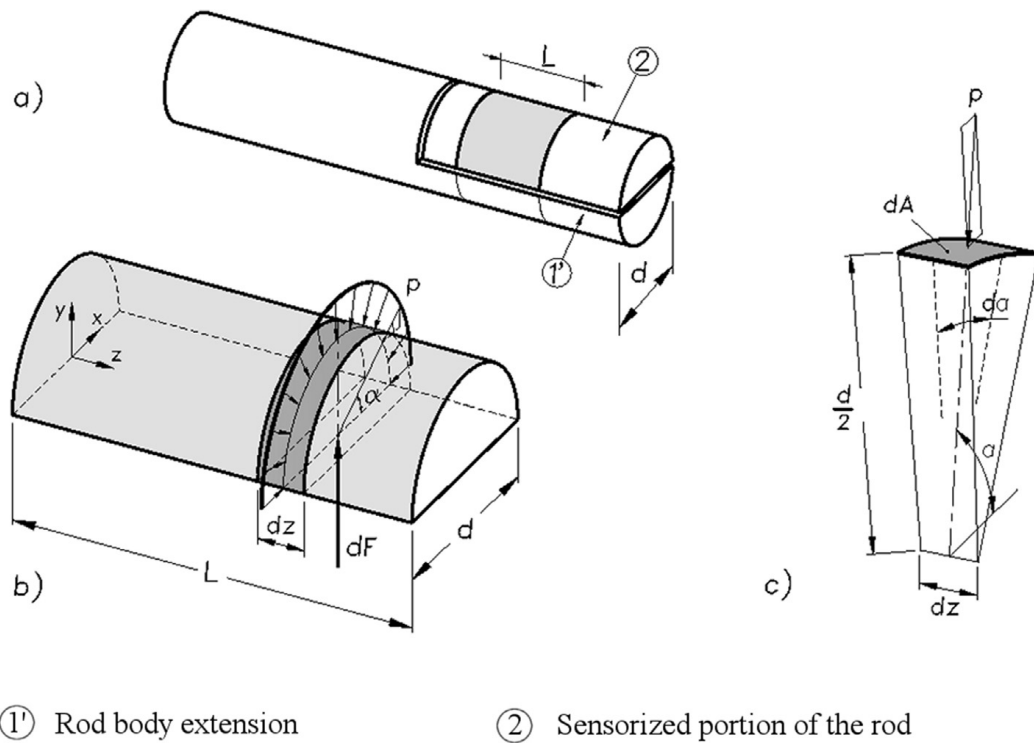
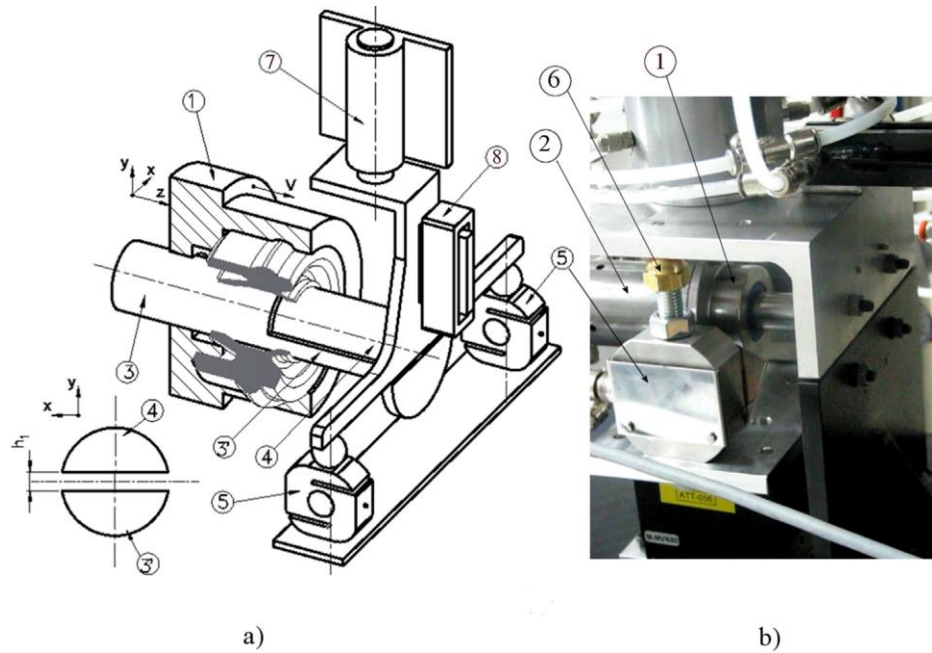


Figure 3.1 a) Sensorized portion of the rod (the full contact area between the seal and the sensorized rod is in grey); b) axisymmetric contact pressure distribution; c) elementary portion of contact area.



- | | |
|---------------------------------|------------------------------|
| ① Seal holder | ⑤ Load cells |
| ② Pneumostatic bearing | ⑥ Precision screws |
| ③ Fixed cylinder rod | ⑦ Pair of pneumatic bearings |
| ③' Rod body extension | ⑧ Pneumatic pad |
| ④ Sensorized portion of the rod | |

Figure 3.2 Sketch a) and photo b) of the measuring portion of the test bench.

3.2 Modification of Test Bench

Some parts of the corresponding test bench were modified according to increasing the accuracy of measuring contacts pressure of lip seal by its interface. To this aim it is better to guaranty the movement of cylinder rod by restricted its movement in the exact direction for preventing additional movements by means of designing two appropriate sliding bearings (Figure 3.3) according to the GGB catalog of bearing technology by using the diameter of the cylinder rod for choosing best characteristics to designing them and other related elements like Pneumostatic cylinder internal seats for the bearings (3.4.1).

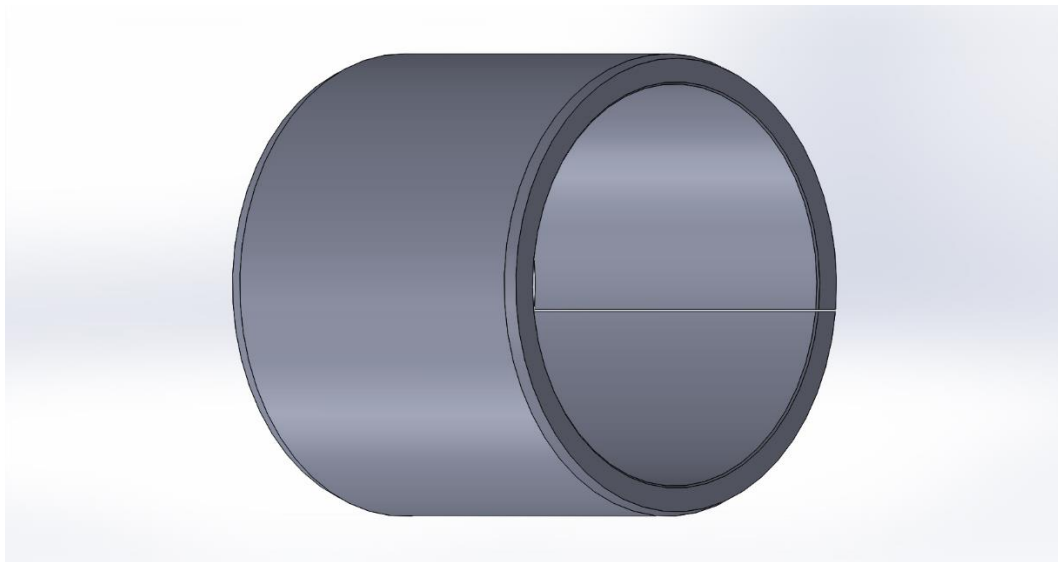


Figure 3.3 sliding bearing

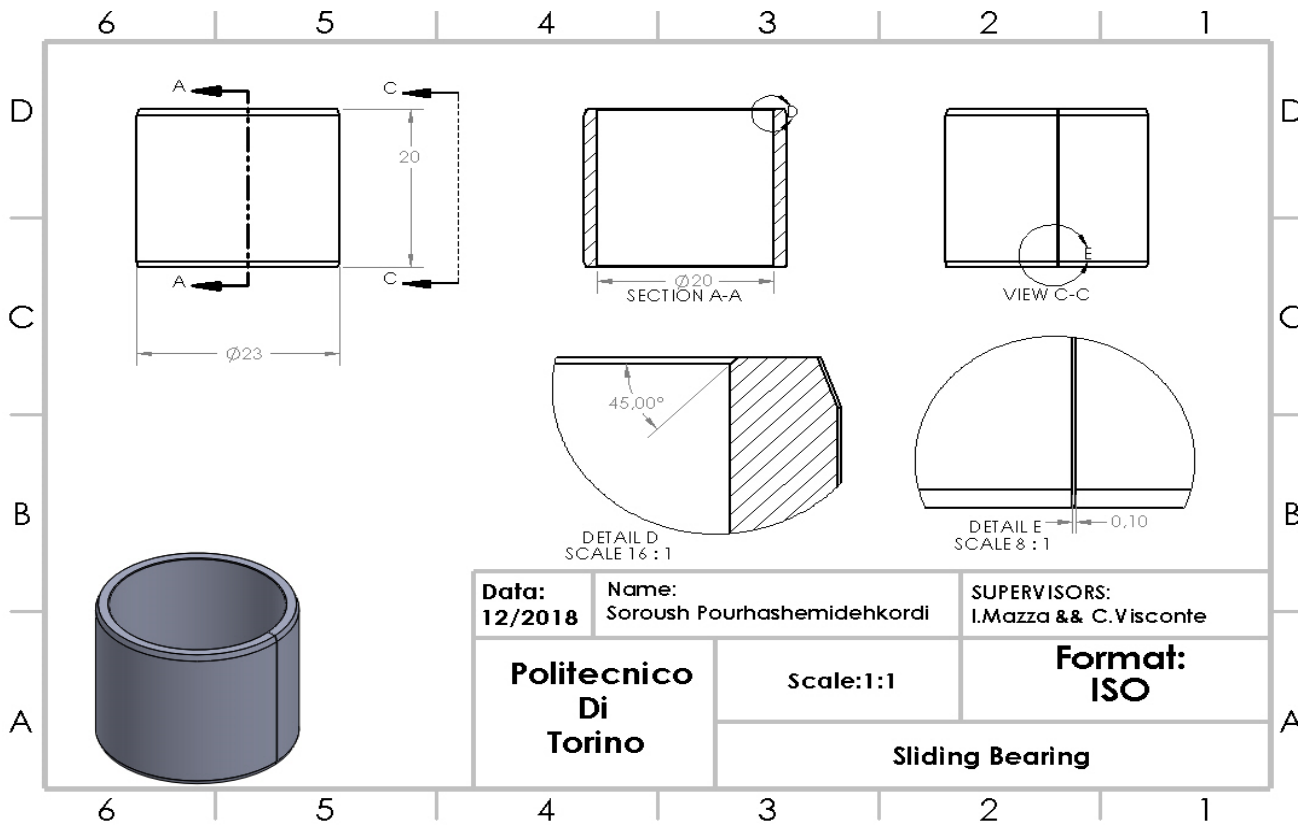


Figure 3.3.1 drawing sliding bearing

Furthermore, the Pneumatic cylinder (Figure 3.4) redesigned without any hole on it, because before the modification the Pneumostatic cylinder had some holes on its body for applying the air on the seal to check whether the corresponding type of seal can prevent the leakage of air on the cylinder or not, But the problem was that the pressure that could be applied to the cylinder was limited by the hole's resistance against the leakage of the air from these holes. Indeed the internal part of the new Pneumostatic cylinder has been changed in order to host 2 sliding bearings and a seal (Figure 3.3); in the following, we will consider this seal.

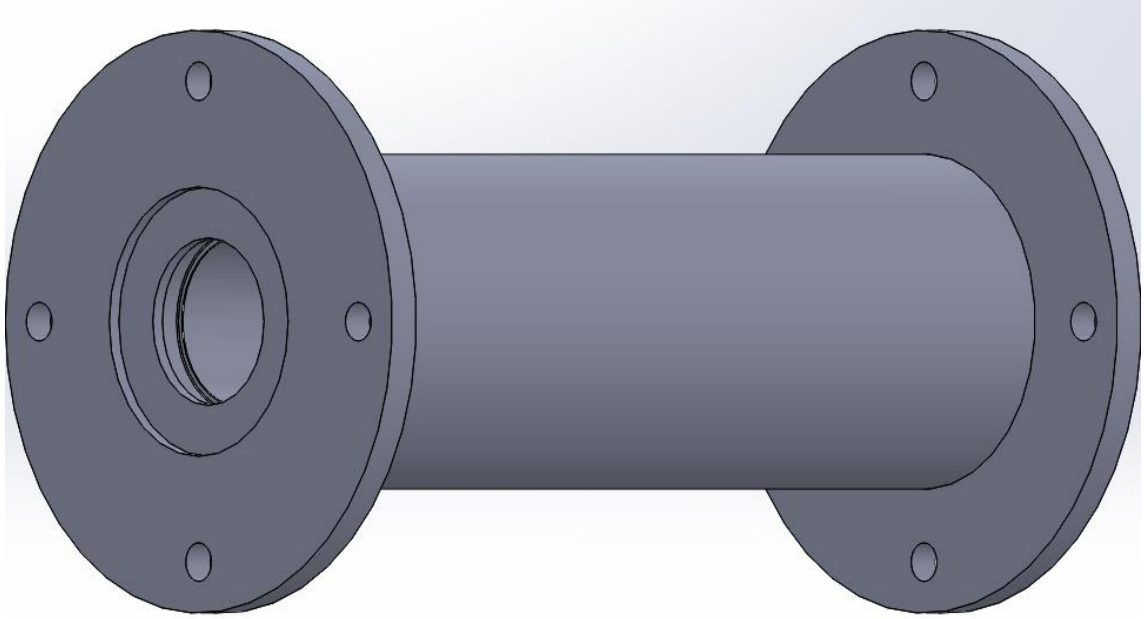


Figure 3.4 Pneumostatic cylinder

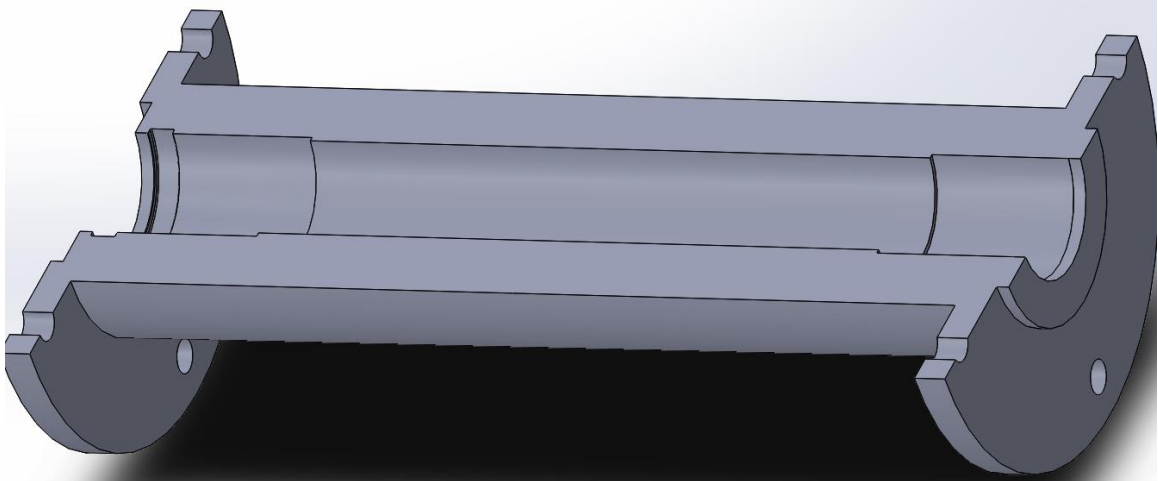


Figure 3.4.1 Pneumostatic cylinder

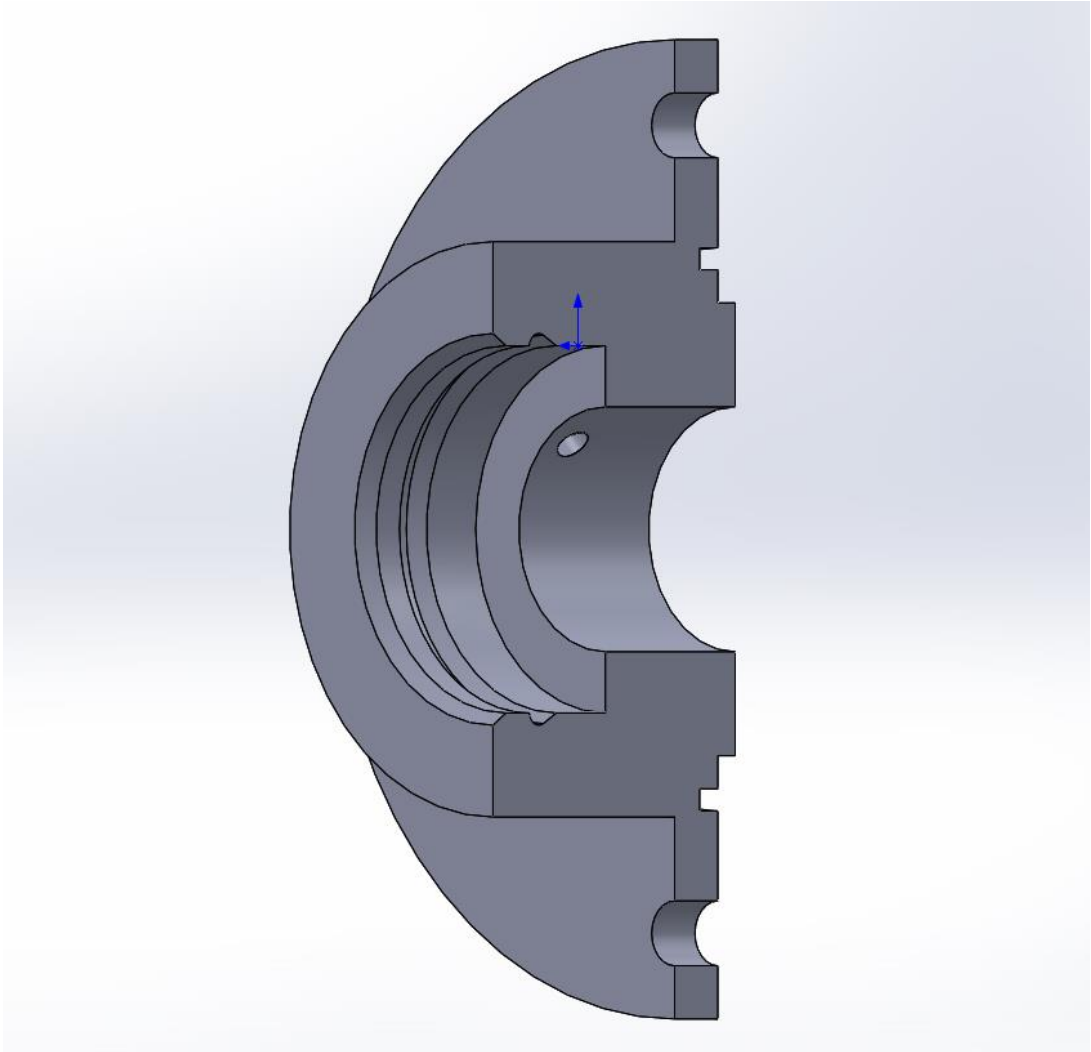


Figure 3.5 Seal holder

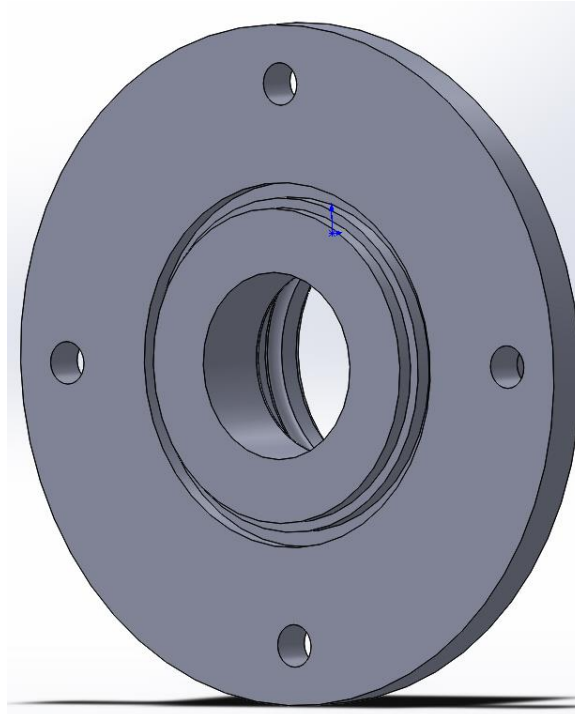


Figure 3.5.1 Seal holder

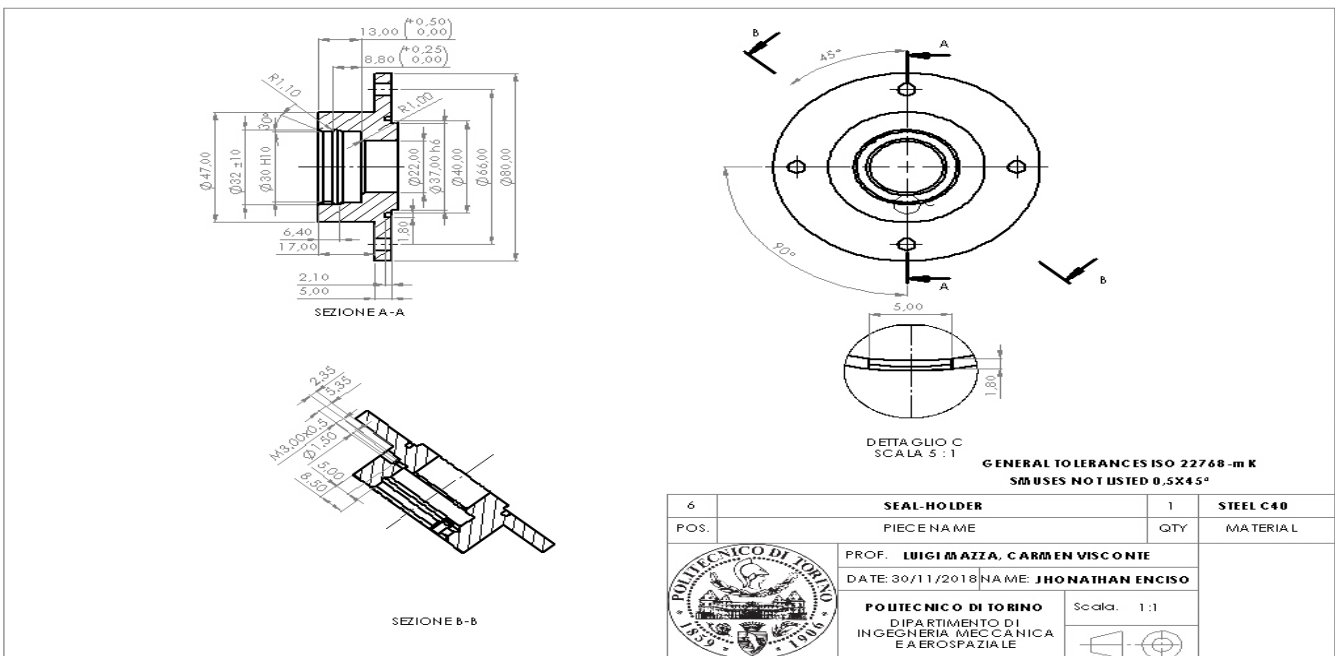


Figure 3.5.2 Drawing Seal holder

In addition, in order to have the availability of pressurizing the seal we need to use a Raccordi (Figure 3.5.3) in the seal holder hole.



Figure 3.5.3 Drawing Seal holder

The final assembly of the modified pieces is showing below:

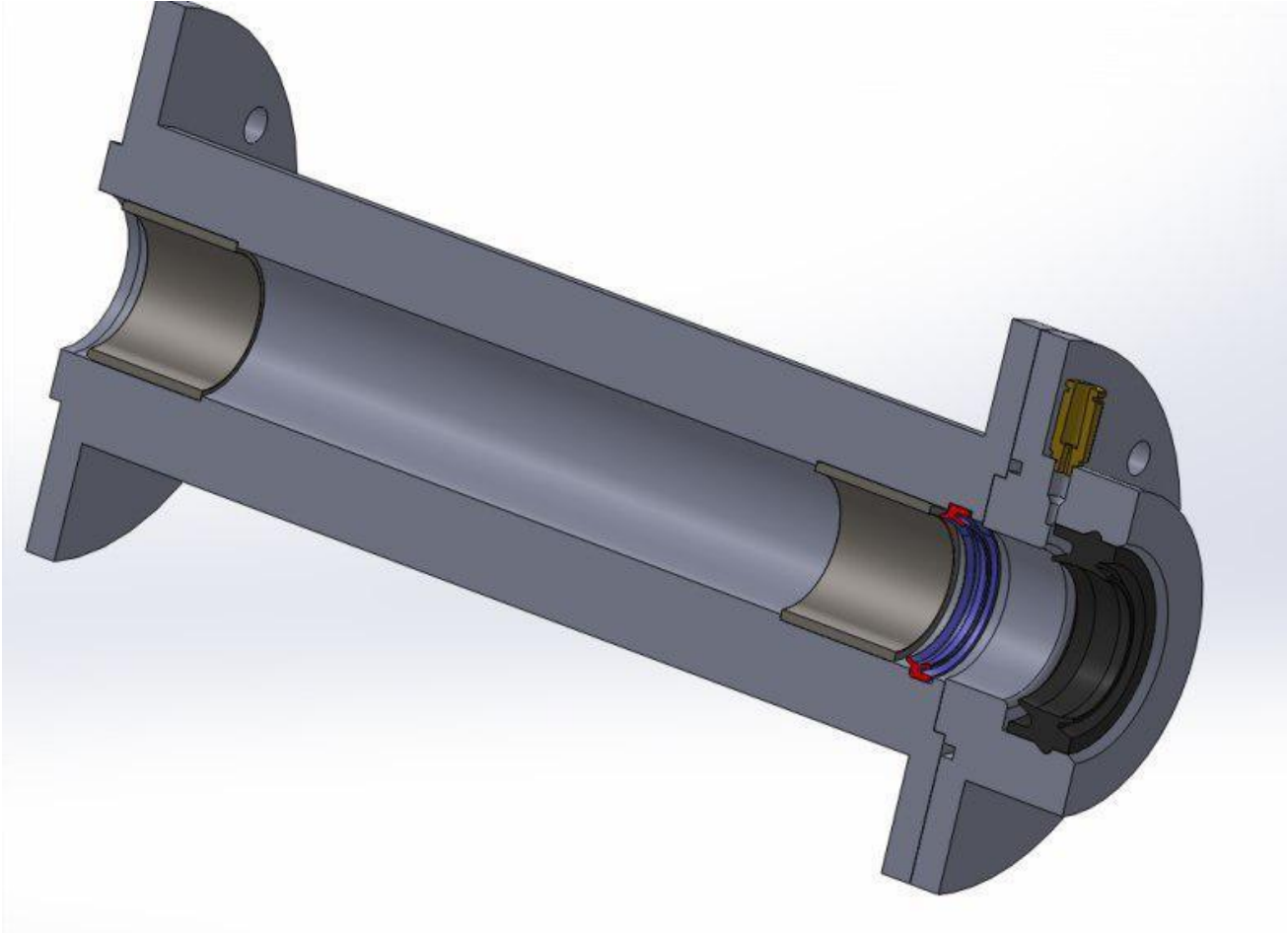


Figure 3.5.3 Assembly of parts

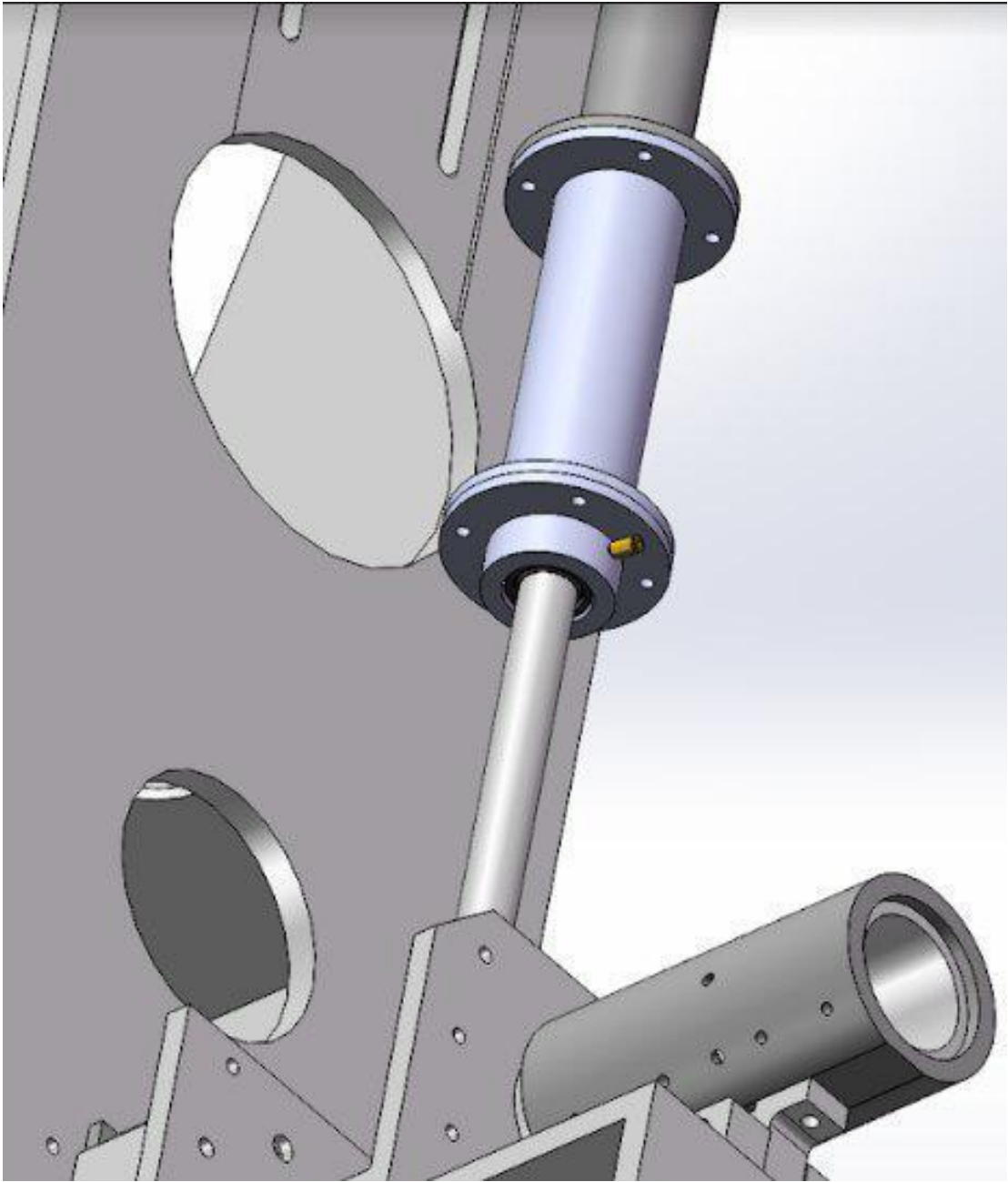


Figure 3.5.3 Test Bench

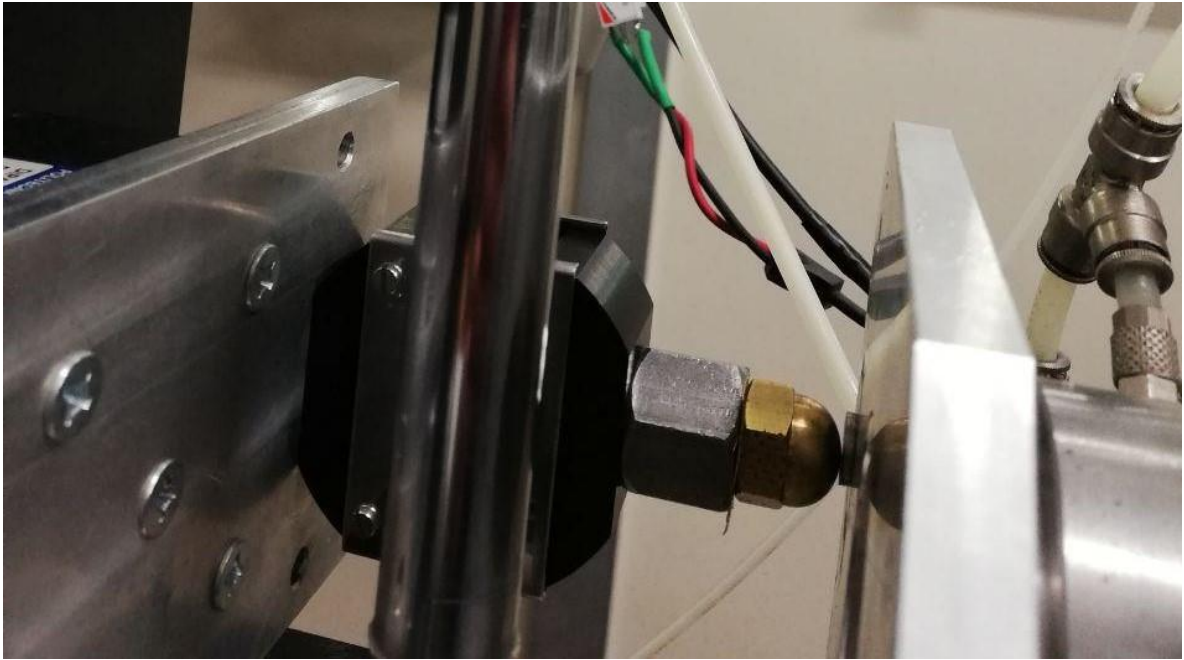


Figure 3.7 Load cell

For capturing and monitoring, the data which we want to derive from the load cell and analyzing them in each test. We used an appropriate acquisition system which it could support 32 channels, but we just used two channel, one for load cell output and another one for the output of the speed sensor. Therefore, it could connect to the PC through the USB and with its specific software, we derived the data.



Figure 3.8 Acquisition system

Another important element which we need it for performing the measurements is the speed sensor which we can regulate its speed for the range of cylinder movement, actually it can control the speed of cylinder for performing the measurements in different velocity conditions, this speed controller has one input and one output which the input is connected to the appropriate supplier and output is connected to the acquisition system.

Also it has a speed regulator switch which with rotating this switch we can change the velocity of cylinder by its wire connection to the cylinder.



Figure 3.9 Speed Sensor

Also for controlling the movements of cylinder in order to push it up and push it down we used two switches to changing the situation of the pneumatics valves which this pneumatic valve contains one input and two outputs that we can change the situation of connection between input and one of the outputs with electrical connection, one of the outputs is connected to the top of the cylinder to push the cylinder down by air and other one is connected to the final part of the cylinder to push the cylinder up.



Figure 3.10 pneumatic valves

This simple controller is connected to the electrical connection of the pneumatic valve which by pressing each one we can change the direction of cylinder movement.

(Picture.9)

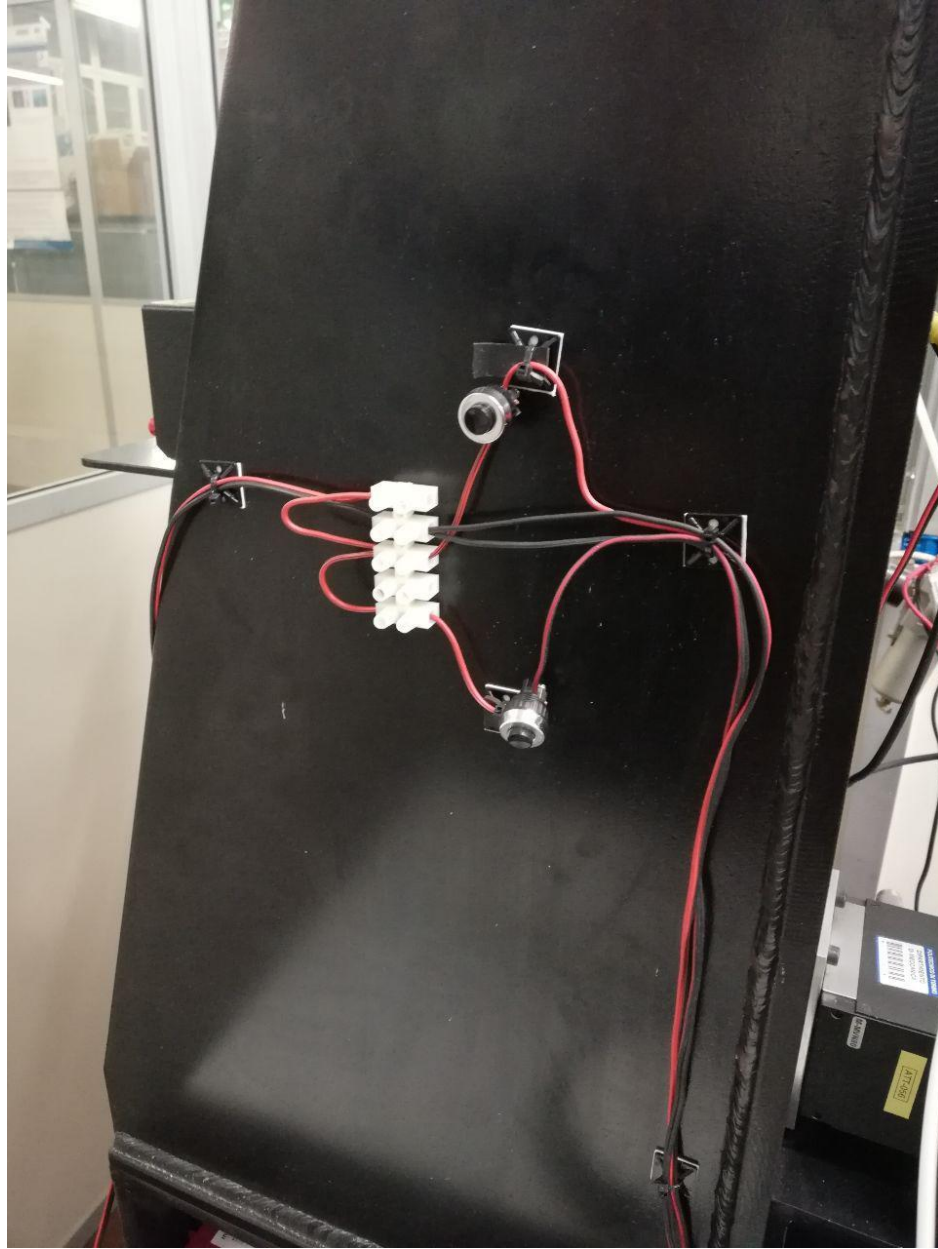


Figure3.11 Electrical controller of pneumatic valve

As previously we illustrated we need some pressures between two seals for testing the two seals in different conditions, so for supplying this portion which is the gap between these two seals with the air we need an air supplier which with rotating its regulator we can increase or decrease the pressure.

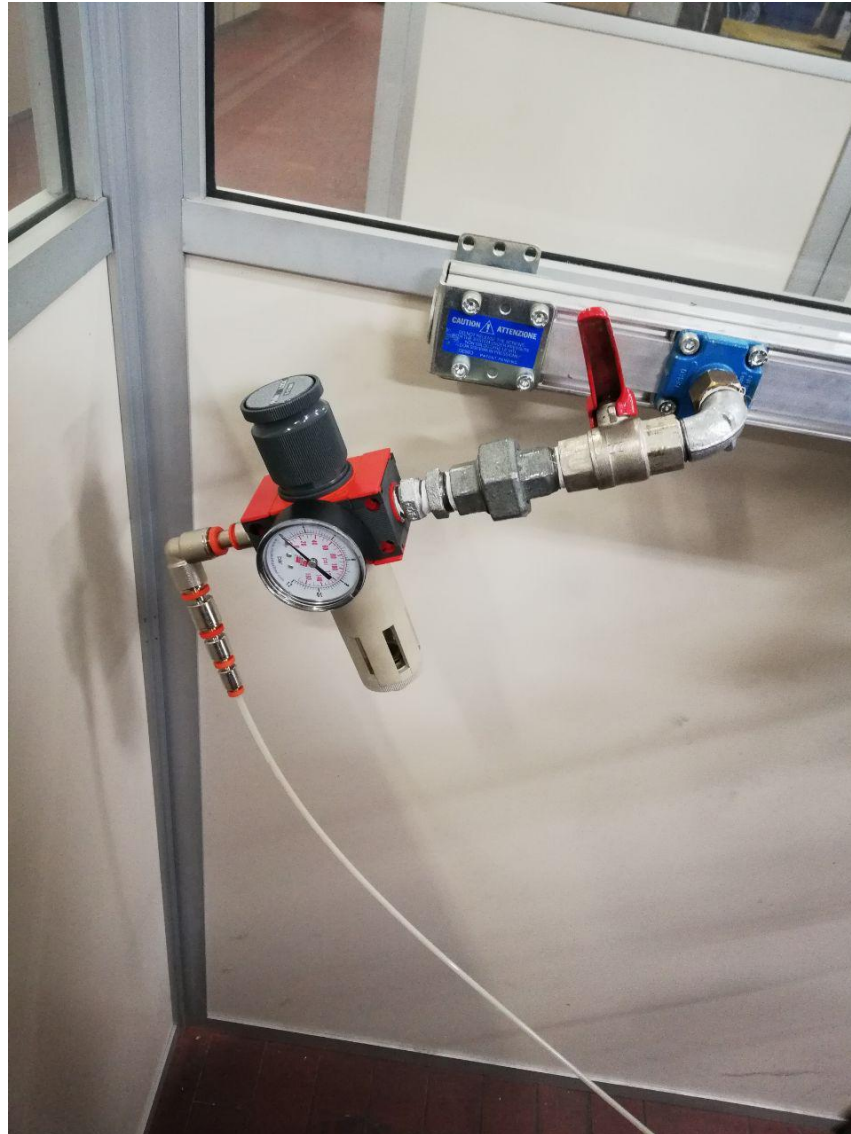


Figure 3.12 Air supplier for seals

For controlling the pressure in this gap area, we have to measure this pressure each time with the appropriate manometer in order to perform accurate tests. In addition, this manometer is connecting to this gap portion.

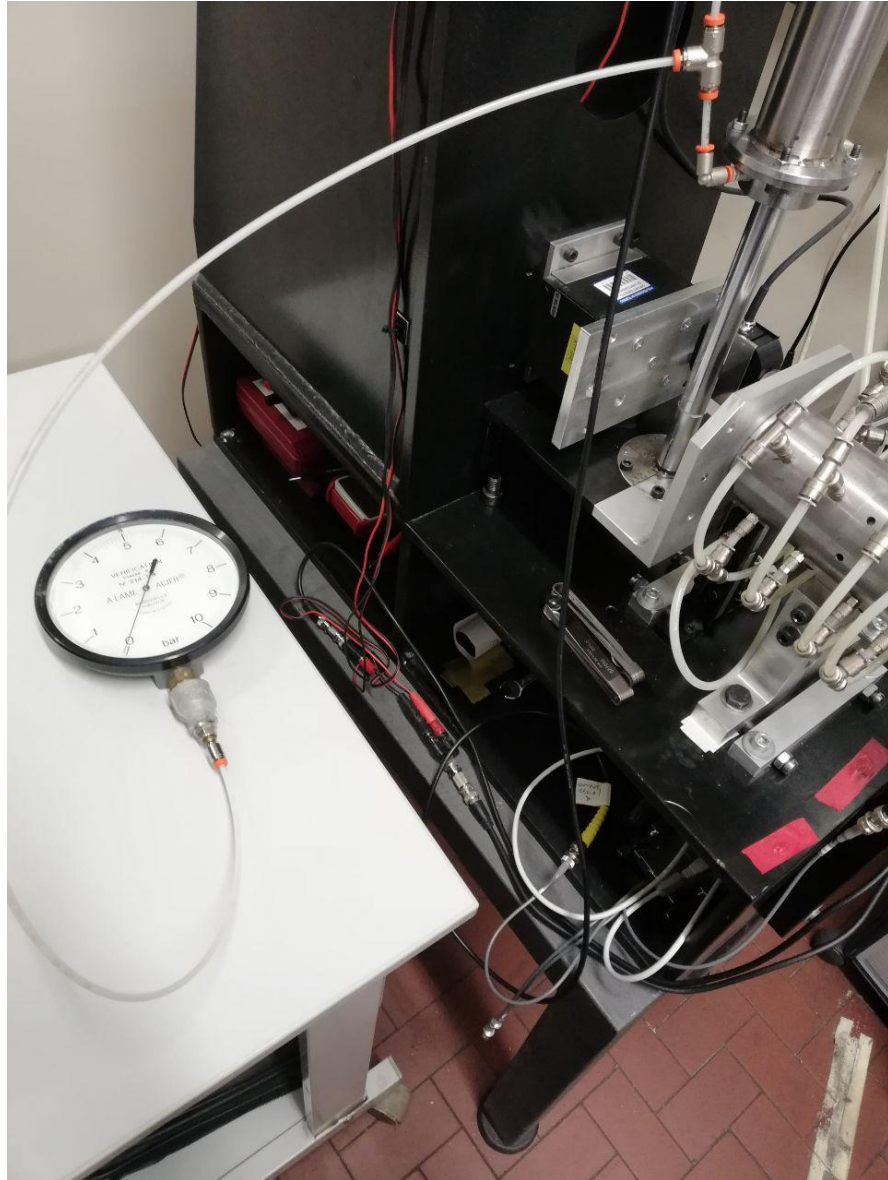


Figure 3.13 Manometer

4.1 Indirect measurement of contact pressure

In order to contribute to a better understanding of the adopted measuring set-up, Fig. 3.2 shows a scheme of the seal assembled on the test bench. The rod seal, which is loaded by compressed air pressure on the left side, is displaced at constant velocity over a fixed cylinder rod (1), whose final portion is split into two sectors: the first one (1') is an extension of the rod body, the second one (2) is free to move in y-direction and connected to two load cells, which are not shown in this scheme. These sensors perform the measurement of the overall radial force oriented in the negative y-direction and exerted by the seal under test on the rod portion (2). To this aim, a gap (3) is provided between the rod sectors, which permits a relative motion without friction. During the test, the seal initially slides over the full rod (Fig. 1a); then, it gradually engages the Sensorized portion of the rod (Figure.4.1); finally, it completely covers the Sensorized rod tip (Figure.4.1) highlights that the radial force measured at a certain instant of time is the resultant of the axisymmetric contact pressure distribution over the corresponding contact area between the seal and the Sensorized rod. While the contact area between the seal and the Sensorized rod tip increases, the sensors detect an increasing radial force until a maximum value is reached. Since the seal motion occurs at constant velocity V , the contact pressure distribution along the z coordinate can be obtained as a function of the force F time derivative, the rod diameter d and the seal velocity V :

$$p(z) = \frac{1}{d} \cdot \frac{dF}{dt} \cdot \frac{dt}{dz} = \frac{1}{d} \cdot \frac{dF}{dt} \cdot \frac{1}{V}$$

Load cell.

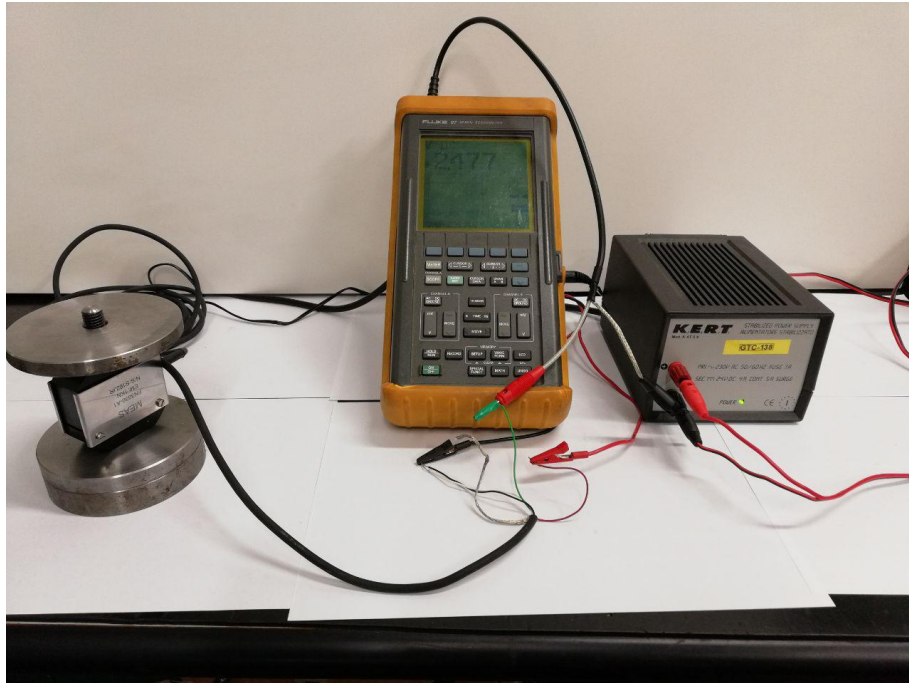


Figure 4.2 calibration setup

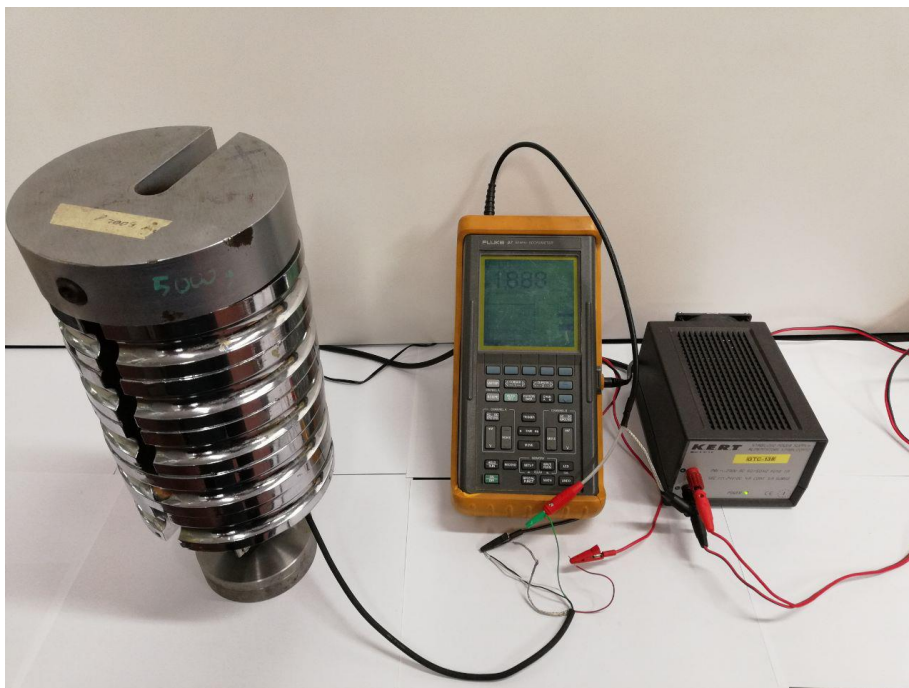


Figure 4.3 calibration setup

In order to increase the accuracy of calibration we performed the tests for three times in both conditions, increase and decrease of the weights, Furthermore the initial weight is the weight of the plate, which is over the load cell.

Voltage Weight	Increase 1	Decrease 1	Increase 2	Decrease 2	Increase 3	Decrease 3
6.1803	2.71	2.707	2.707	2.713	2.714	2.711
55.2303	2.612	2.61	2.611	2.616	2.615	2.612
104.2803	2.516	2.513	2.513	2.518	2.517	2.515
153.3303	2.417	2.413	2.424	2.42	2.417	2.417
202.3803	2.319	2.316	2.324	2.322	2.319	2.319
251.4303	2.22	2.218	2.224	2.224	2.226	2.222
300.4803	2.122	2.122	2.128	2.128	2.124	2.124

Table 4.1 Load cell data

In order to find the calibration, offset we have to obtain the trend of weight versus voltage, then we can drive the trend equation and by decreasing these values from the final voltage which we will drive from the test bench through the acquisition system we can find the offset values. So in order to find this trend we have to find the mean values of three test of both condition of increasing and decreasing for each weight.

$$V_{inc} = \frac{\sum_j^7 \sum_i^3 V_{i,j}}{3}$$

$$V_{Dec} = \frac{\sum_j^7 \sum_i^3 V_{i,j}}{3}$$

Voltage Weight	Average of Increase	Average of Decrease
6.1803	2.710333	2.710333
55.2303	2.612667	2.612667
104.2803	2.515333	2.515333
153.3303	2.416667	2.418
202.3803	2.319	2.319833
251.4303	2.221333	2.223333
300.4803	2.124667	2.124667

Table 4.2 Load cell data

Then by taking the average value of both condition of increasing and decreasing we can obtain the exact trend.

$$V_{Av} = \frac{\sum_j^7 \sum_i^2 V_{i,j}}{3}$$

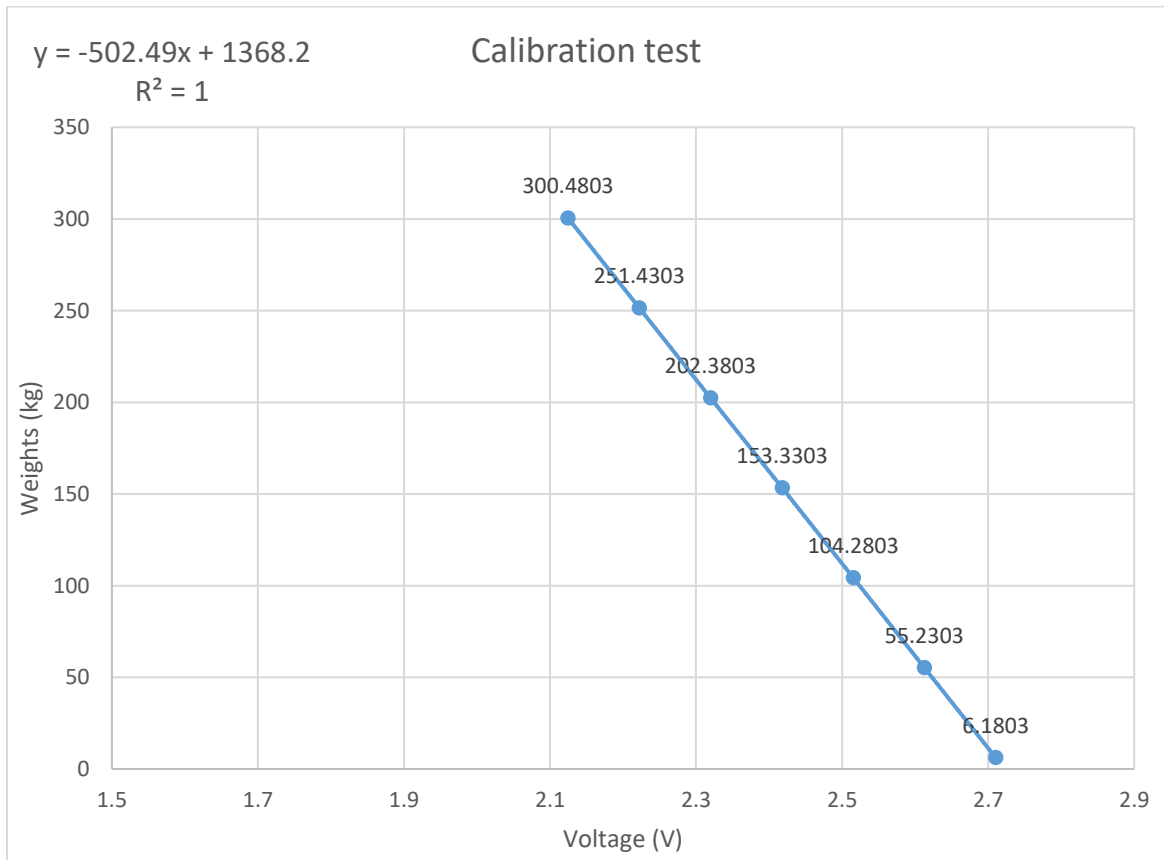


Figure 4.4 Calibration Test

1-5 Experimental Procedure

After preparation of test bench, by connecting the acquisition system to the PC we can start to monitor and recording the data by appropriate software of acquisition system. by setting the software to our initial condition we can start to measuring the voltages of test bench and then through the MATLAB we did the mathematical calculation and filtering data then analyzing the contact forces and eventually contact pressure. Below you can see the experimental procedure.



Figure 5.1 Experimental Procedure

2.5 Starting the Test

In order to starting test procedure first we will open the air through the system to 5 (Bar) to pressurize the air bearing and cylinder, then by turning on the electrical suppliers and then we will regulate the speed of the test and by connecting the Pc to the Acquisition system we are ready to starting the test. Accordingly, in each test condition we will repeat the test at same condition for three times to be sure about the correctness of data, as below you can see we will perform the tests in these conditions.

Main conditions:

1-constant velocity around 1 (mm/s) and variable pressures up to 6 (Bar)

2-Constant pressure around 6 (Bar) and variable velocity up to 100 (mm/s)

Pressure (Bar)	0	2	4	6
Velocity(mm/s)	1	1	1	1

Table 5.1 Test conditions

Pressure (Bar)	6	6	6	6
Velocity(mm/s)	5	10	50	100

Table 5.2 Test conditions

Pressure	6 Bar	6 Bar	6 Bar	6 Bar	6 Bar	6 Bar	6 Bar
Velocity	1 mm/s	1 mm/s	1mm/s	2 mm/s	2 mm/s	5 mm/s	5 mm/s
Frequency	200 Hz	500 Hz	1 KHz	1 KHz	2 KHz	1 KHz	2 KHz

Table 5.3 Test Conditions

Then by switching the cylinder movement controller by changing the position of connection between inputs and outputs, we will push the cylinder down by means of air pressure on the cylinder.

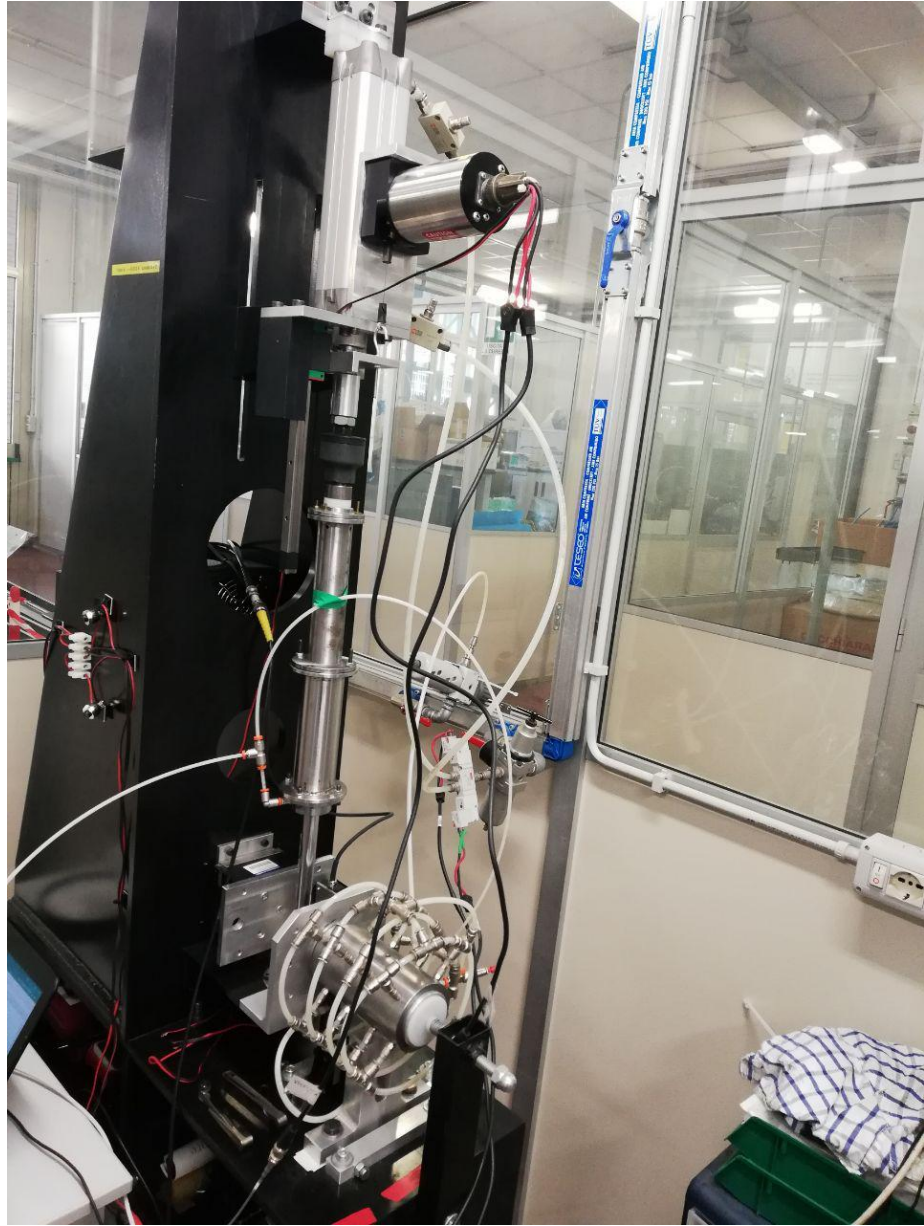


Figure 5.2 Complete Test Bench

2.5 Recording data

Instantly when the cylinder starts to moving downward by starting to monitoring the velocity through the software we would be sure about the correctness of velocity, then by approaching the cylinder to the divided portion of road we will start to recording the data and we will wait until the full stroke happen and then by stopping the recording we can say the first test is finished and by pressing the controller switch we will force the cylinder goes up by this plan we can performs all the tests and then by extracting the data from the software and transform them to the next step.

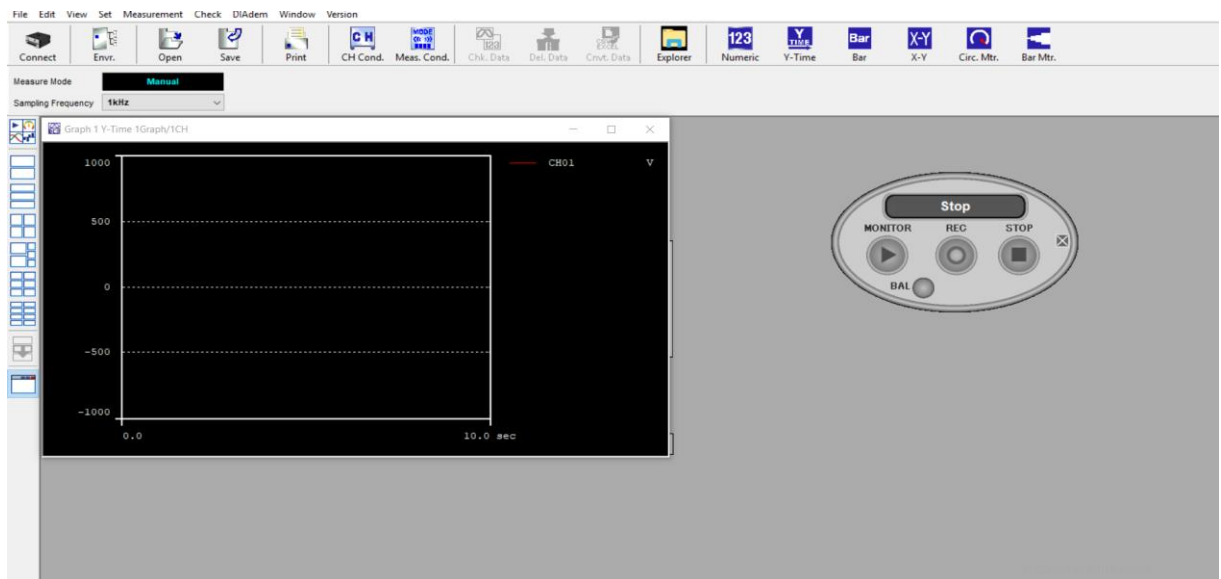


Figure 5.3 Software area

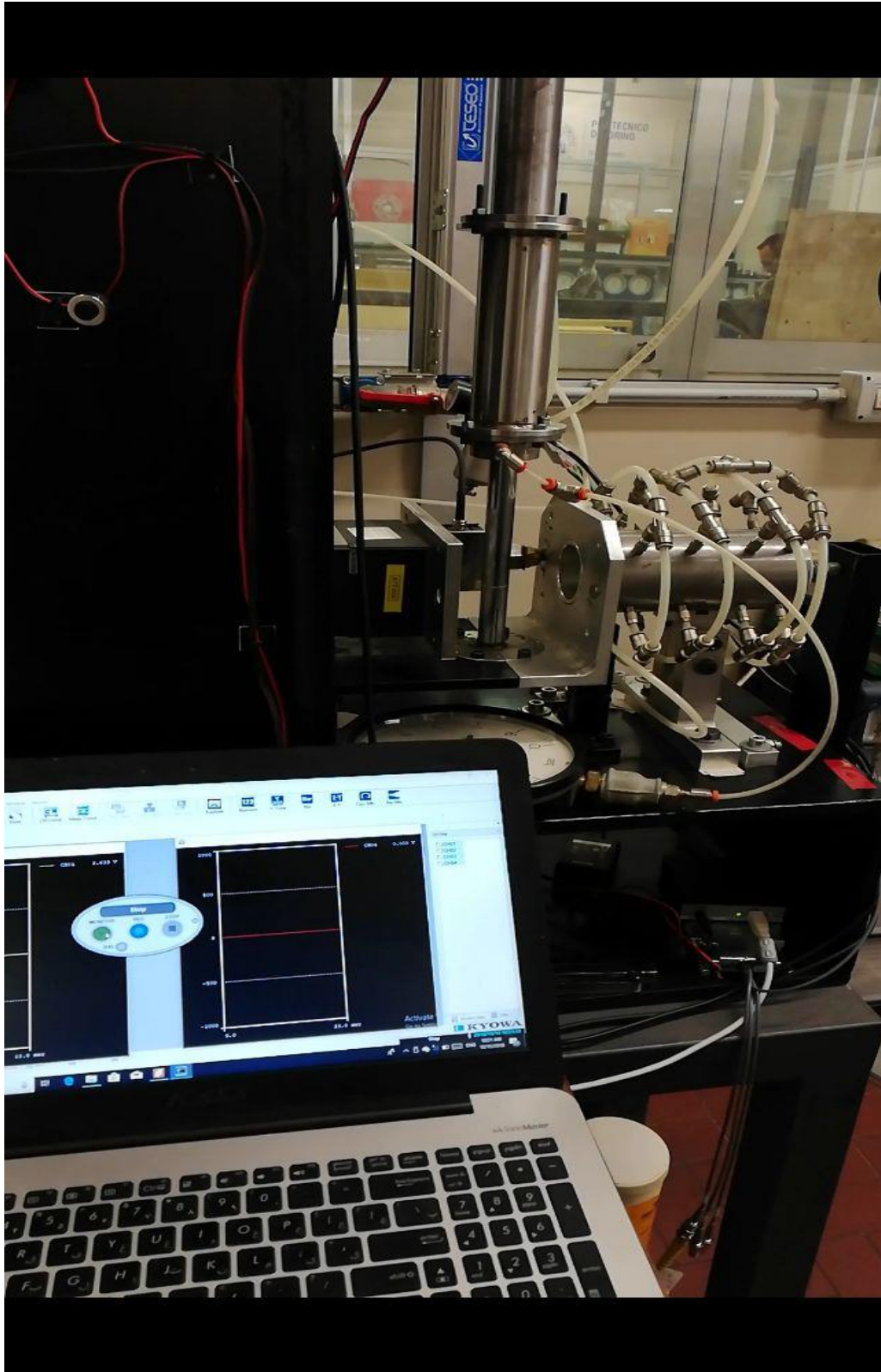


Figure 5.4 Test Procedure

3.5 MATLAB

In order to performing the needed mathematical procedure, we will be importing the derived test results from the Acquisition system to the Matlab area and then to add filter for decrease the noises of the system we will work on the Simulink.

First we will be initializing the data files to the Matlab command for each test condition, then we will introduce each test file as a matrix with 3 columns and N

row which first column is the Time of the test long, the second column is the Voltage data of the load cell and the third column is the velocity data from the speed sensor, after initializing the initial values we will substitute the calibration values which we found previously to the second column of each test condition then we will decrease the initial force that the load cell will be applying to the system during the measurements, then the difference of this two value is our force data and is ready to import to Simulink to perform our goals.

3.5.1 Matlab Procedure

In the Matlab command as you can see we called the tests files as File1, File2 and File3, then as we explained previously we divided each column of Files and by performing the calibration value we found our force versus time like u3, u6 and u9.

```
15 %%                               %% Initialization
16 - clc
17 - clear all
18 - close all
19 - % addpath('test\Test (Velocity=1,Pressure=6) ');
20 - File1=xlsread('Test0011.xls');
21 - File2=xlsread('Test0012.xls');
22 - File3=xlsread('Test0013.xls');
23 - T1=File1(:,1);
24 - u1=(File1(:,2).*-502.5+1368.2);
25 - u2=(mean(u1(1:100)));
26 - u3=u1-u2;
27 - u4=(File2(:,2).*-502.5+1368.2);
28 - u5=(mean(u4(1:100)));
29 - T2=File2(:,1);
30 - u6=u4-u5;
31 - T3=File3(:,1);
32 - u7=(File3(:,2).*-502.5+1368.2);
33 - u8=(mean(u7(1:100)));
34 - u9=u7-u8;
```

Figure 5.5 Matlab Command

For instance, u3, u6, and u9 obtained from the difference of voltages which derived from the load cell and multiplied by the calibrated value (-502.5+1368.2) and the mean value

of the initial values which derived by the load cell that explained before due to the internal mechanical parts in the rest position.

For example, this is a force diagram of pressure equal to (2 Bar) and velocity (1mm/s):

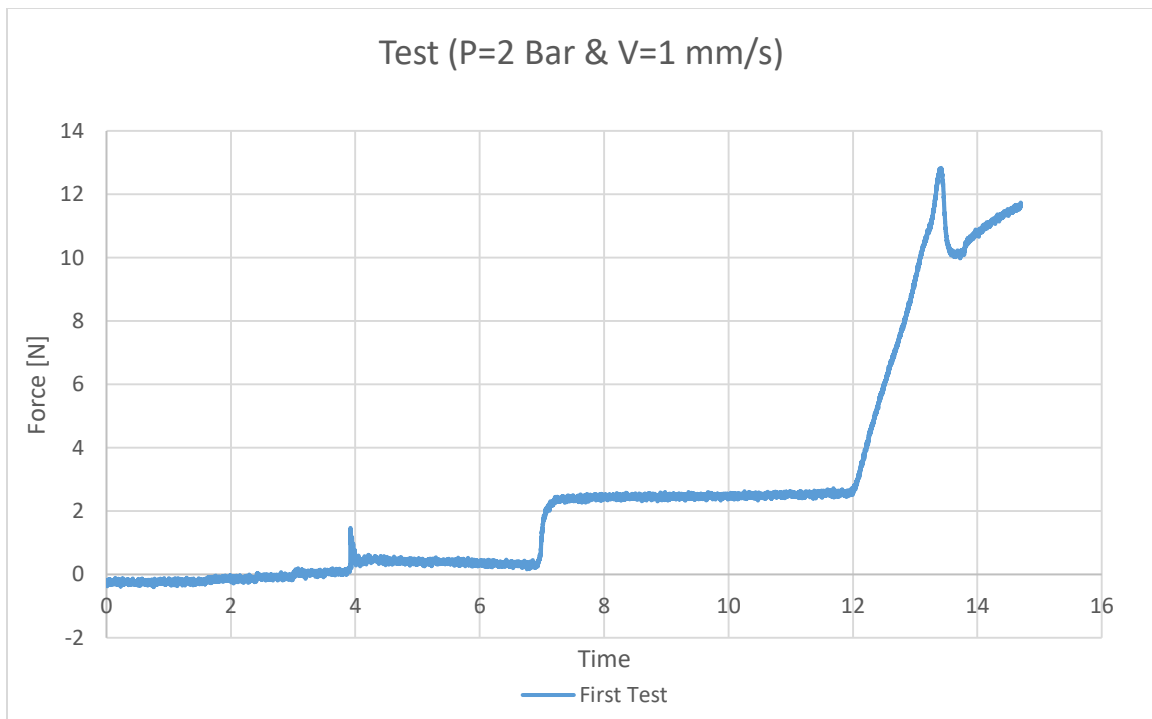


Figure 5.6 Force Plot

According to perform a test with high percentage of accuracy the tests was performed three times which the shape of their figure is almost same but their starting points are not equal and for this reason we have to obtain their starting points to synchronizing three test starting points for obtain their mean figure of three test.

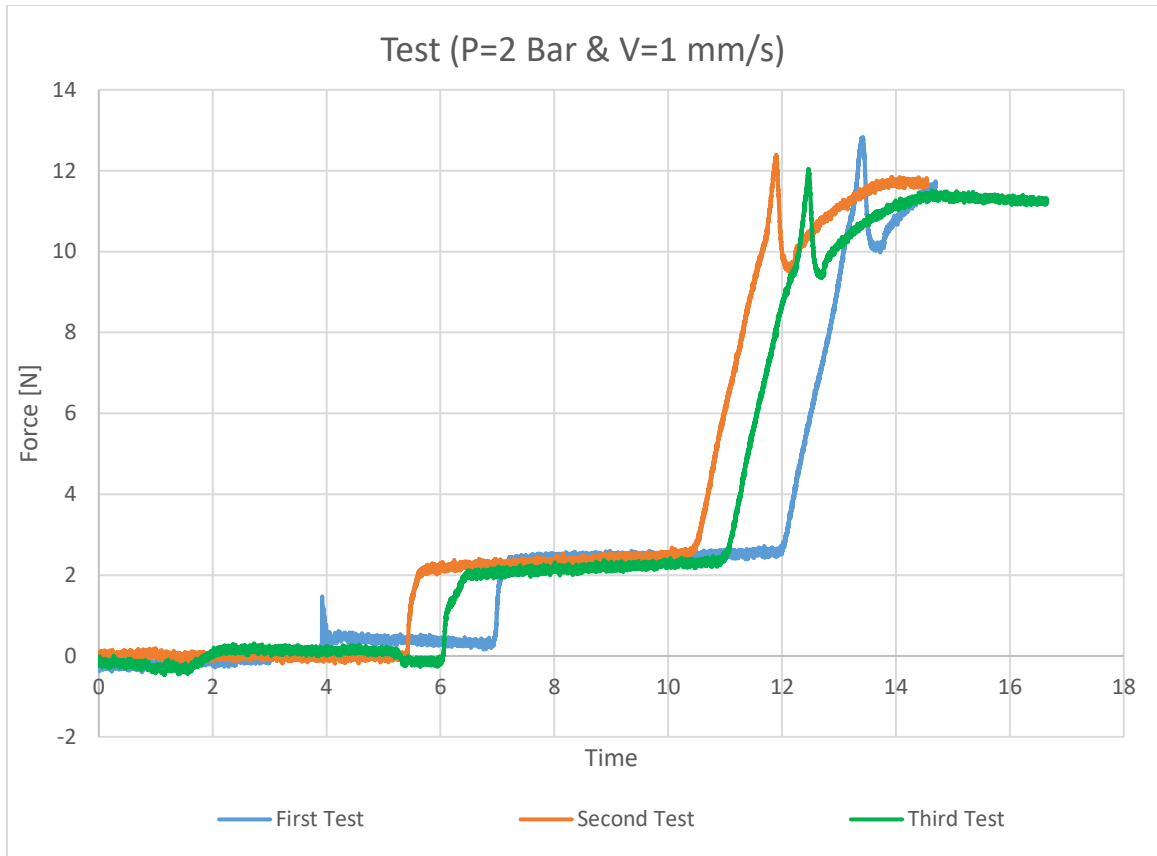
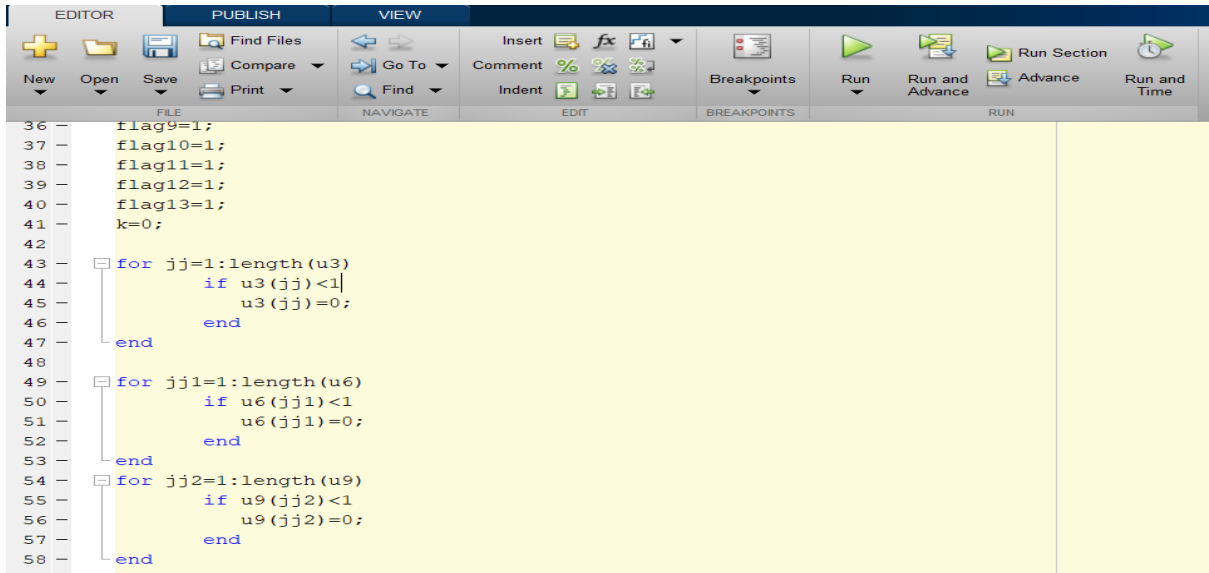


Figure 5.7 Three test figure together before synchronizing

In order to find their starting points an appropriate threshold was specified which could be variable related to the condition, here specified as 1 (N) and by the condition that specified in the for loop, it would put zero all the data less than 1 (N).



```
36 flag9=1;
37 flag10=1;
38 flag11=1;
39 flag12=1;
40 flag13=1;
41 k=0;
42
43 for jj=1:length(u3)
44     if u3(jj)<1
45         u3(jj)=0;
46     end
47 end
48
49 for jj1=1:length(u6)
50     if u6(jj1)<1
51         u6(jj1)=0;
52     end
53 end
54 for jj2=1:length(u9)
55     if u9(jj2)<1
56         u9(jj2)=0;
57     end
58 end
```

Figure 5.8 Three for loops for finding the starting points

Then we have to find the last zero of each figure before starting point by means of using a part of command to find the exact mean value of each figure then by turning back and checking where is the first zero, which is the starting point of the figure for reaching to this condition some Flags are specified 1 and when the condition will have satisfied will turn to zero.

```
61 -  
62 - while flag8  
63 -     k=k+1;  
64 -     if u3(k)>=mean(u3)  
65 -         flag8=0;  
66 -     end  
67 -     y=k;  
68 - end  
69 - k1=y;  
70 - while flag9  
71 -     k1=k1-1;  
72 -     if u3(k1)<=0  
73 -         u3(k1)=0;  
74 -         flag9=0;  
75 -     end  
76 -  
77 -     y1=k1;  
78 - end  
79 -  
80 - k2=0;  
81 - while flag10  
82 -     k2=k2+1;  
83 -     if u6(k2)>=mean(u6)  
84 -         flag10=0;  
85 -     end  
86 -     y2=k2;  
87 - end
```

Figure 5.9 Matlab command

In the next step after defining the starting points now, we have to understand which one is bigger than other by specifying some condition we can understand the priority of each one compared to the other then we desired to put the last one as a reference and shifted back to other to synchronizing three figure in the same starting point.

```

115 - end
116 -
117 - false=1;
118 - false1=1;
119 - false2=1;
120 - while false
121 -     if y1>=y3 && y3>=y5
122 -         X=y1-y5;
123 -         X1=y3-y5;
124 -         u3=u3(X:end);
125 -         u6=u6(X1:end);
126 -     end
127 -
128 -     if y1>=y5 && y5>=y3
129 -         X=y1-y3;
130 -         X1=y5-y3;
131 -         u3=u3(X:end);
132 -         u9=u9(X1:end);
133 -     end
134 -     false=0;
135 -     break;
136 - end

```

Figure 5.10 Matalb command

This is the figure of three force after synchronizing in the same starting point:

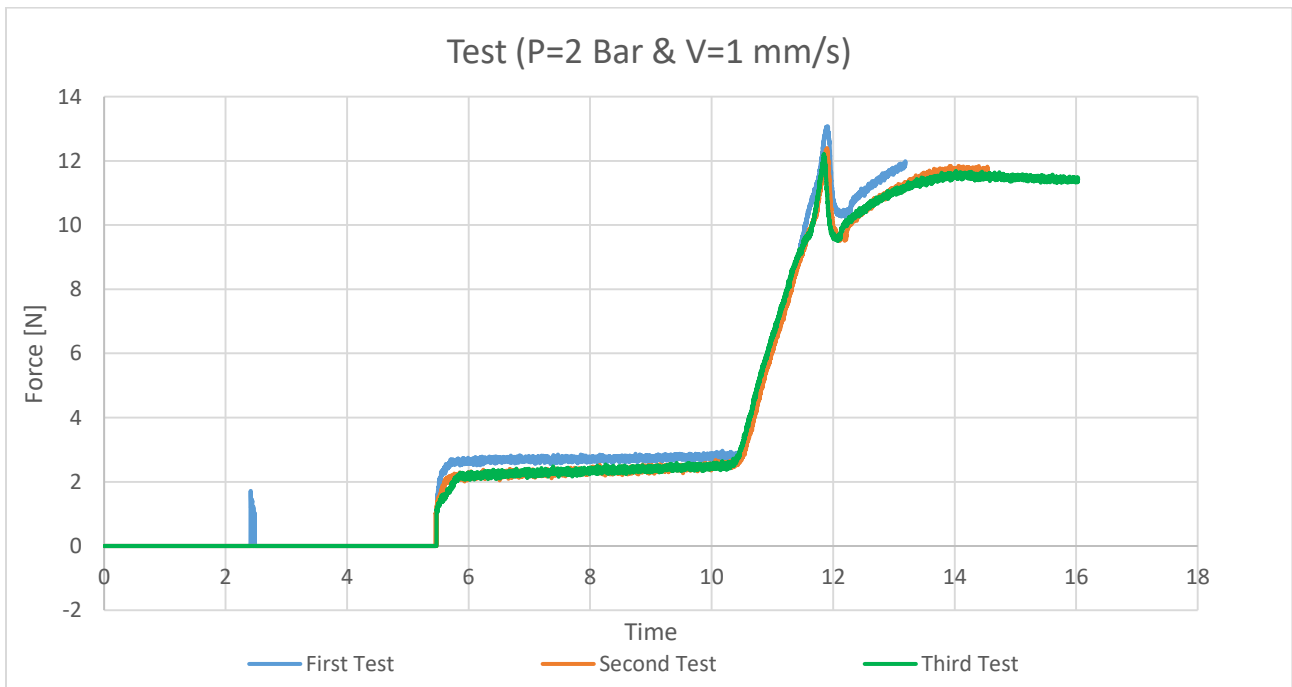


Figure 5.11 Three force at the same starting points

Then by obtaining the Median force matrix of three forces by summing three matrices and dividing by three, then the mean value of the velocity of each test and the total median of three-velocity V_{av} will obtain, by the same procedure the T_{av} matrix also will obtain.

Median and T_{av} are the inputs of the Simulink by means of command Sim (name of Simulink model) and block from workspace we can transfer the desired data from Matlab to Simulink.

3.5.2 Simulink

After performing these staffs, we will open the Simulink part and adding a block for calling the force value as an input for our subsystems, then by applying an analog low pass filter block we can filter the noises of the system.

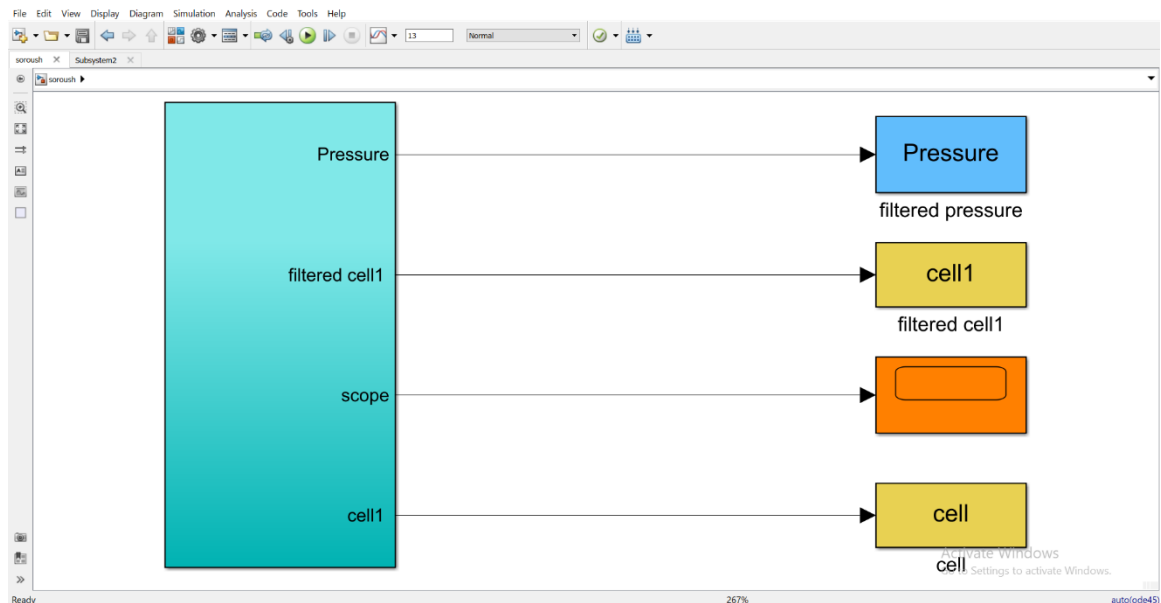


Figure 5.12 Total model in Simulink

3.5.2.1 Analog Filter

According to our condition, we decided to choose the Fourth order of the Butterworth low pass filter for filtering the noises to have clear data and much near as near to the original data. Butterworth filters [3] have good amplitude and transient behavior.

Furthermore, for filtering the force signal we choose its passband edge frequency in the range of [5-100] (rad/s).

3.5.2.2 Different Type of Analog Filters

Butterworth Filter

The Butterworth or maximally flat magnitude filter has a flat (mathematically as much as possible) frequency response. The analog low pass filter's (Butterworth) 'brick wall', which can be defined as standard approximations for various filter orders are shown in the below figure (including ideal frequency response).

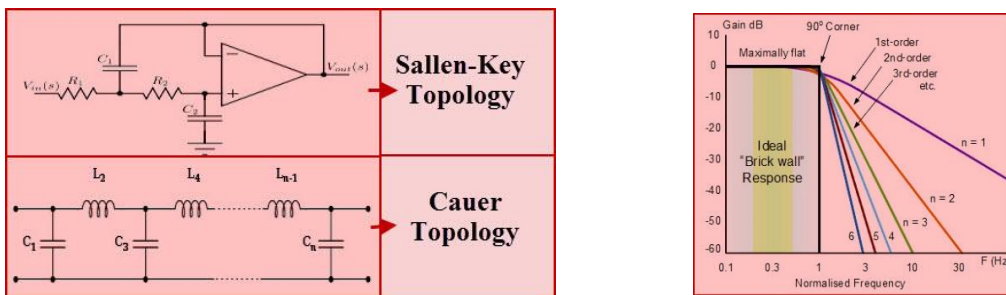


Figure 5.13 Filter design and frequency response

If we increase the order of the Butterworth filter, then the Butterworth filter design cascaded stages also are increased. Thus, as shown in the above figure the filter and brick wall response gets closer. Generally, the linear analog filters are realized using various topologies, the Butterworth filter can be realized using Cauer topology or Sallen-key topology.

Chebyshev Filter

The Chebyshev filters are named after Pafnufy Chebyshev who derived the mathematical calculations of Chebyshev filters. The error between the characteristic of idealized filter and actual filter can be reduced using the property of Chebyshev filter.

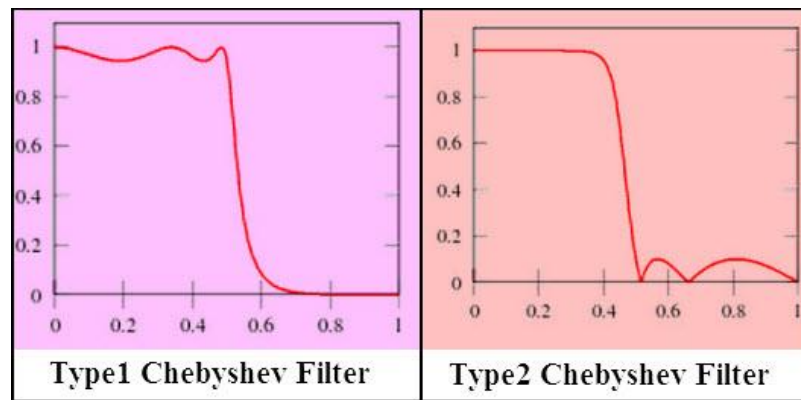


Figure 5.14 Chebyshev Filter frequency response

These Chebyshev filters are further classified as type1 and type2 Chebyshev filters. The type1 filters are basic type and the gain or amplitude response is an angular frequency function of the nth order of analog low pass filter (LPF-if we consider analog filters). The type2 Chebyshev filter is an uncommon type and is an inverse filter.

Bessel

The Chebyshev filters improve on the amplitude response at the expense of transient behavior. The Bessel filter is optimized to obtain better transient response due to a linear phase (i.e. constant delay) in the passband. This means that there will be relatively poorer frequency response (less amplitude discrimination).

By performing the Bessel filter, we obtained a clear signal compared to the original signal:

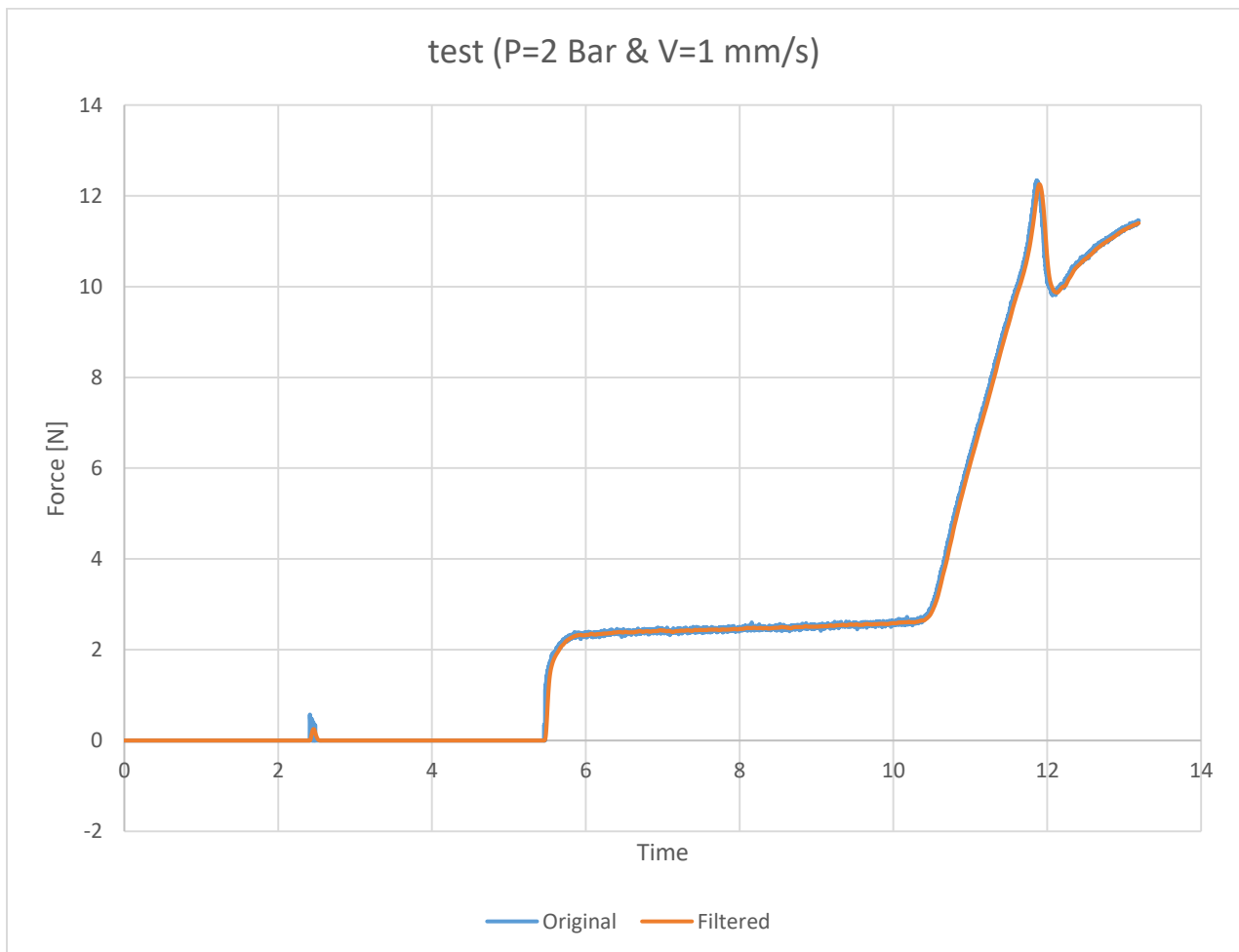


Figure 5.15 Original Signal compared to Filtered signal

Then we have to perform first derivative of the force, which the input is the force and the output is the contact pressure by using the formula, which below you can find it, It is the first derivative of force which multiplies by the one over of velocity (1mm/s) and diameter of the rod which is 20 (mm).

$$P(Z) = \frac{1}{d} \cdot \frac{dF}{dz} \cdot \frac{dt}{dt} = \frac{1}{d} \cdot \frac{dF}{dt} \cdot \frac{1}{v}$$

In the figure which represented in the below is the process of performing the upper formula to reach the contact pressure.

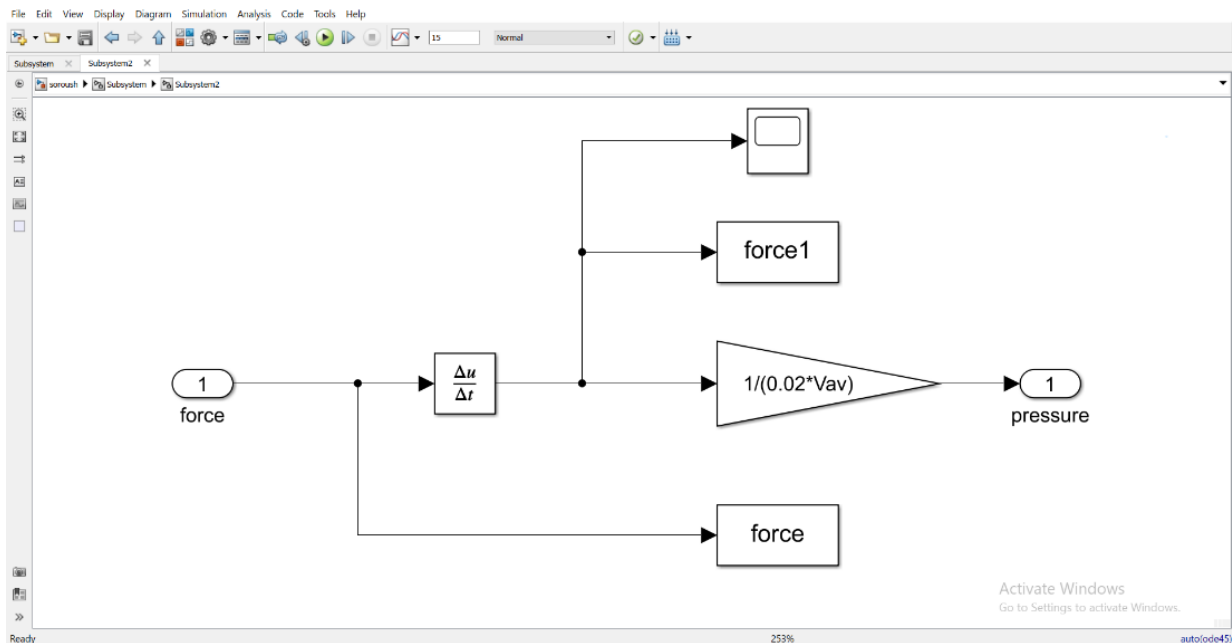


Figure 5.16 Simulink

The by filtering the output which is pressure we have the final pressure; indeed, we do not have negative pressure by performing the function block which could cancel the negative data.

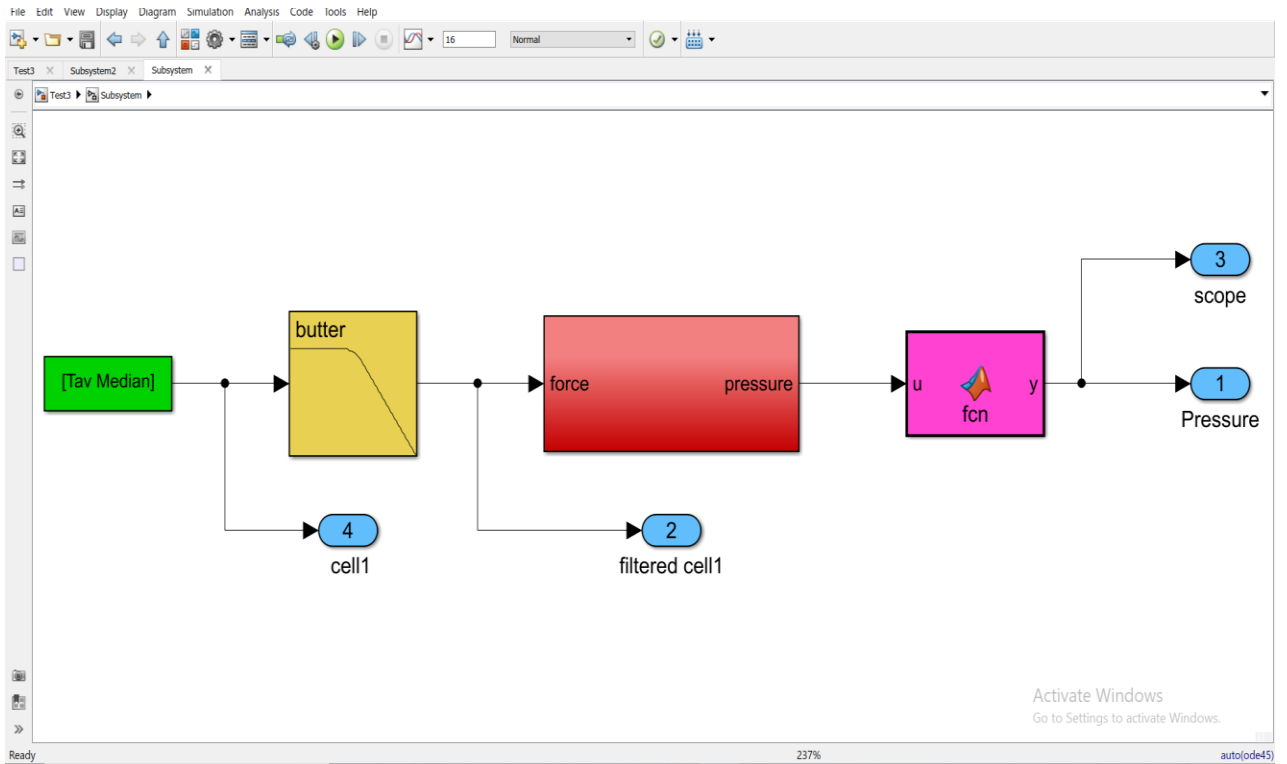


Figure 5.17 Hole Simulink model

Then by transferring the final pressure to the Matlab we can perform some operation in order to do some corrective actions on the pressure figure.

This figure is before performing correction:

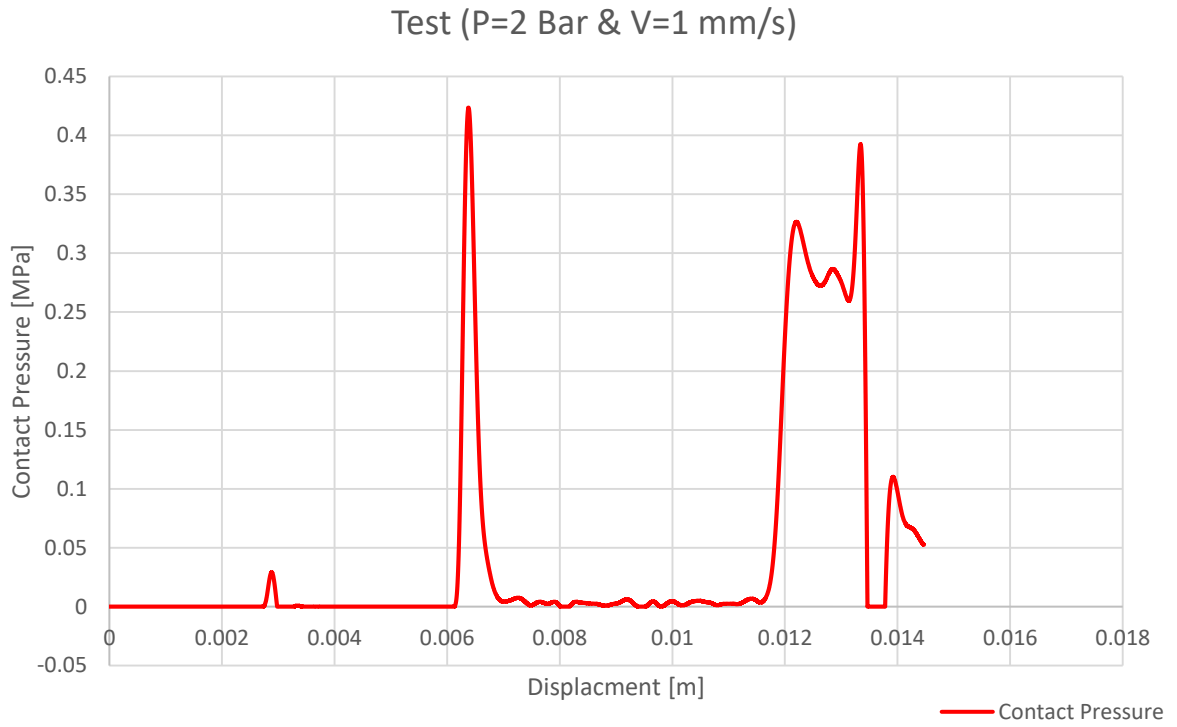


Figure 5.18 Contact Pressure versus displacement

This figure is after performing correction on the contact pressure:

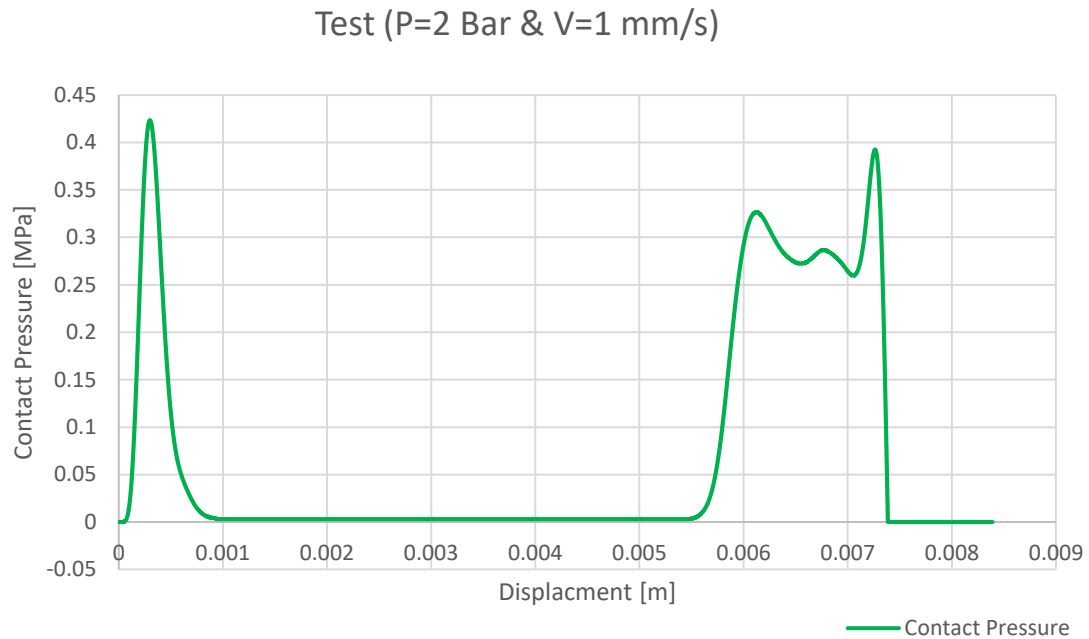


Figure 5.19 Contact Pressure versus Displacements

For obtaining the displacement, we have to multiply the velocity by time ($Z = V \times T$).

According to the tests, condition that previously explained we would have these final figures as below you can see in two categories, one at same velocity with variable pressure and another at same pressure with variable velocity.

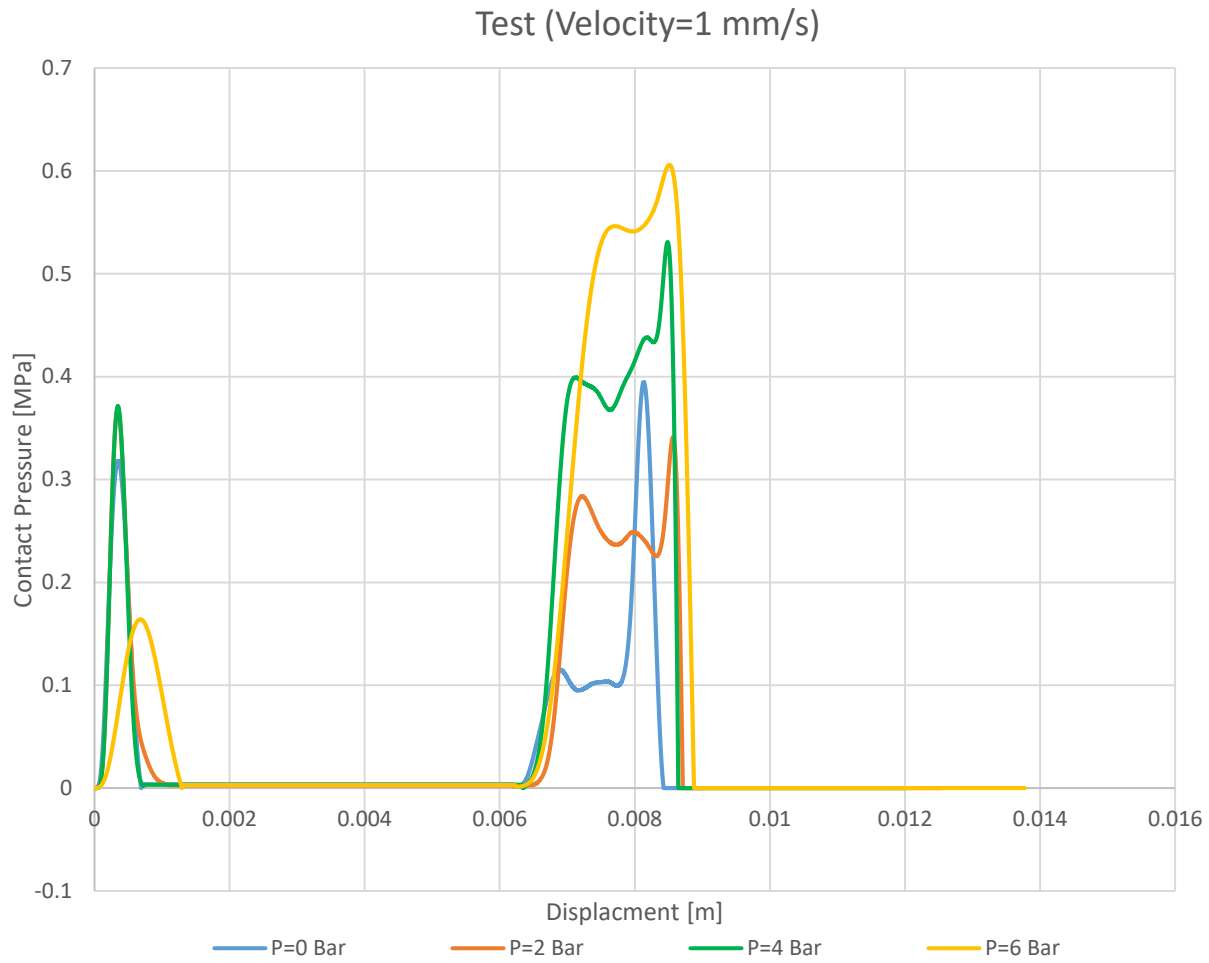


Figure 5.20 Contact Pressures at same velocity with different pressure

Test (Pressure=6 Bar)

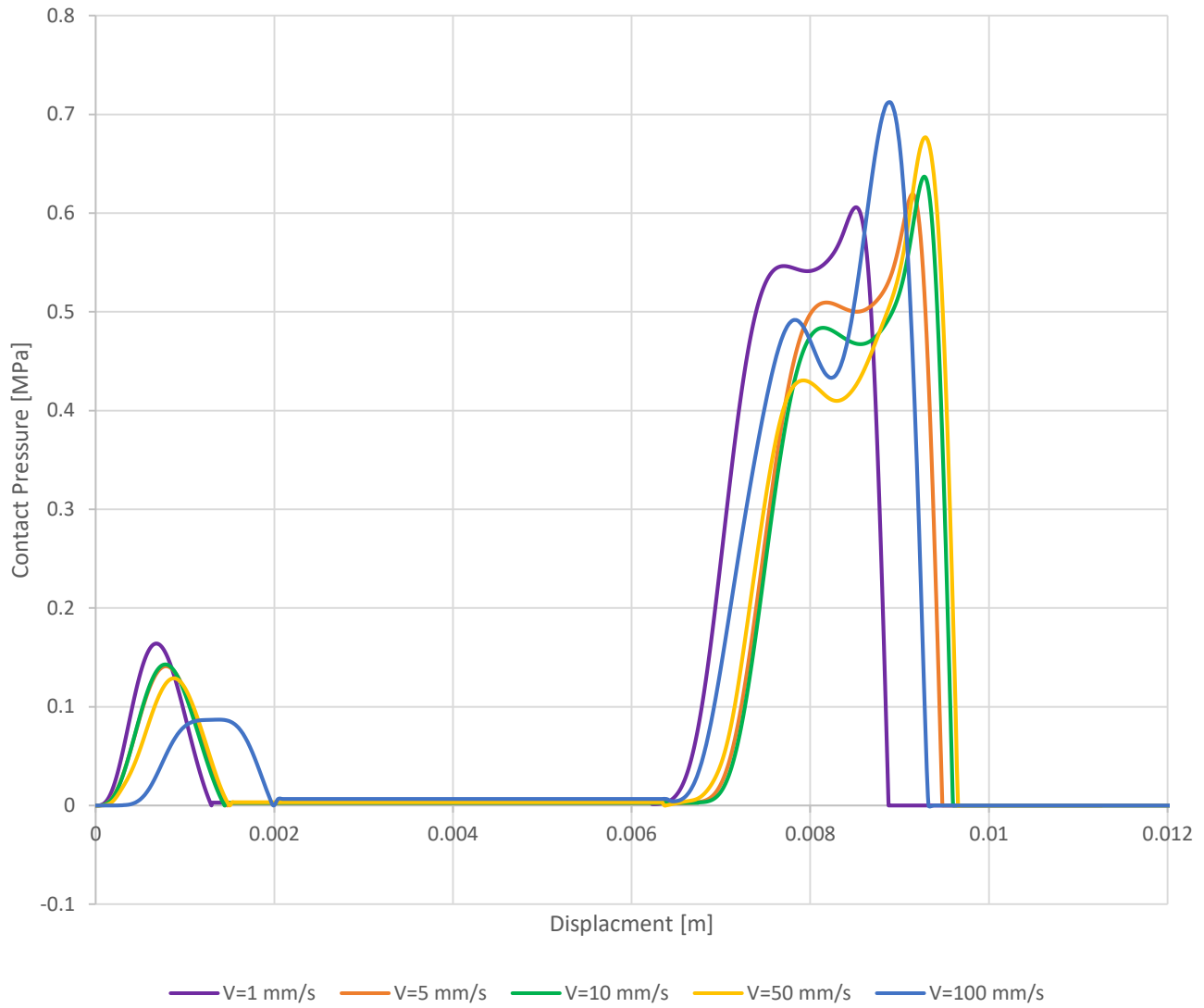


Figure 5.21 Contact Pressures at Different velocity

Test (Pressure=6 Bar)

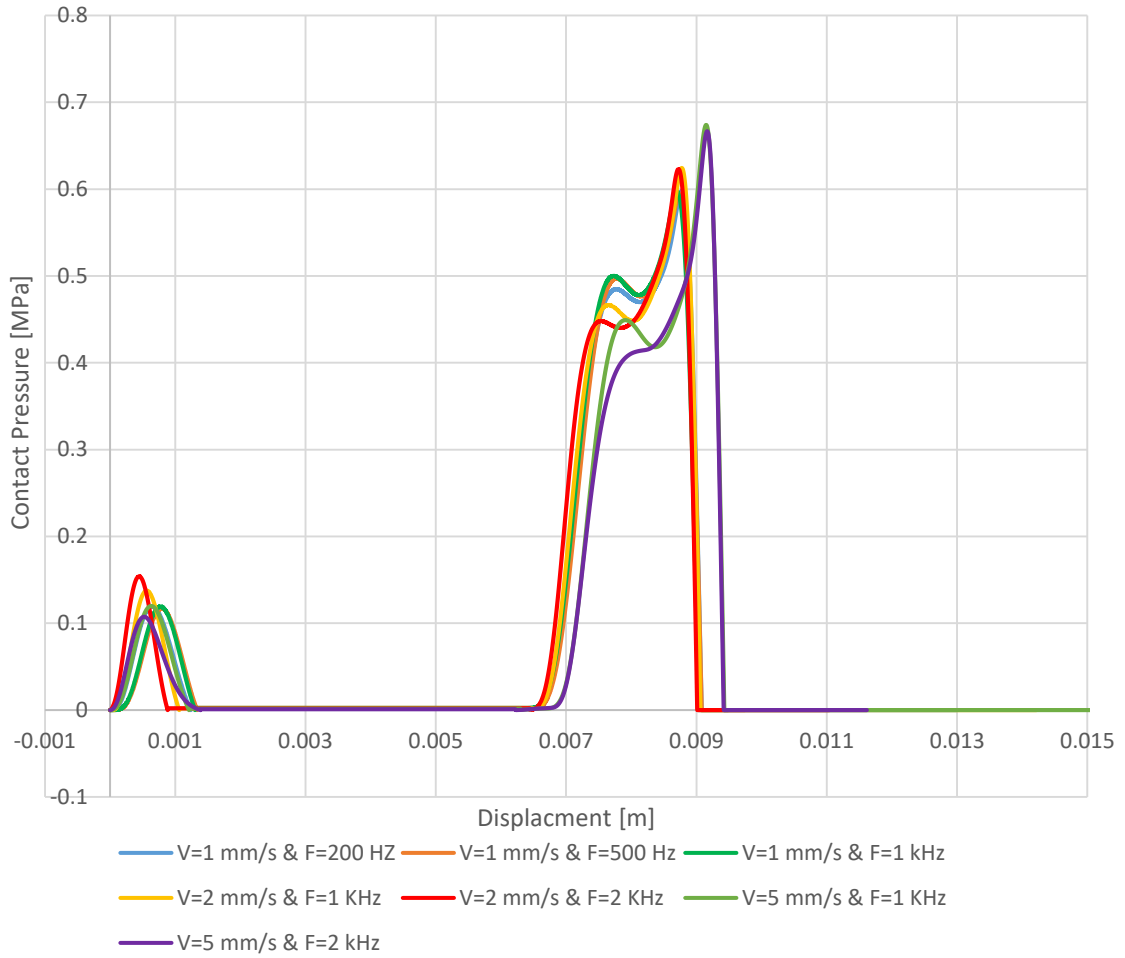


Figure 5.22 Contact Pressure in different frequency

4.5 Analyzing Test Results

Actually, Figure (5.20) shows the experimental result of first tests condition which is in the variable pressure and constant velocity, The first picks are from the first lip of the seal, which they are not pressurized, In the constant velocity with different pressure you can see they are almost same in the point of contact pressure value and displacement, but Figure (5.21) shows the second test condition which is variable velocity with the constant pressure. And Figure (5.22) shows the effect of changing the frequency in the same condition and different conditions, As you can see with changing of frequency the behavior of the system is not so different and we can neglect it.

The idea is analyzing the second pick of contact pressure because it is related to the second lip seal, which is pressurized. Indeed, you can see in the constant velocity with increasing the pressure the contact pressure also will increase but we can say the displacement is constant but with increasing the velocity, the behavior of second pick also is changing that by increasing the velocity the amount of contact pressure is decreasing.

Conclusion

Results of experimental tests aimed at the evaluation of contact pressure at the interface between an elastomeric rod seal for pneumatic cylinders and its metallic counterpart are presented. Tests were carried out using a specifically modification of test bench that is able to detect the radial force exerted by the rod seal displaced at different test conditions on a sensorized portion of a cylinder rod over time. Pressure load can be applied on the seal to reproduce actual working conditions. No intrusive measuring device was interposed between the tribological couple, which is the main advantage of the presented method. On the other hand, the test bench assembling requires a special care and parts alignment must be done

accurately. Certainly, the displacement of the sensorized portion of the rod needed to generate the radial force signal could affect the contact pressure measurement. Nevertheless, the choice of high stiffness load cell in a parallel assembly ensures a maximum displacement of less than $1\ \mu\text{m}$ at the highest value of measured force. On the other hand, the possibility of a small intrusion of the wiper lip into the gap between the fixed cylinder rod and its sensorized portion could be a limit of the proposed test bench.

Experimental results, which gave the radial force trend over time, were post processed through Matlab to indirectly calculate contact pressure distribution. In particular, the radial force signal was filtered by specific butterworth filter. In this way, the radial force signal could be differentiated and contact pressure distribution was computed as a function of the radial force time derivative, the seal velocity and the rod diameter. Preliminary results

obtained on a type of rod lip seal for pneumatic actuators are presented. The experimental test bench and the computational methodology described are general and can be applied to pneumatic rod seals with geometries and materials other than that described in this study. Future work would be addressed to the evaluation of the influence of different working conditions and to the development of a numerical model to compare results.

References

- [1] Bignardi C, Manuello A, Mazza L. Photoelastic measurements and computation of The stress field and contact pressure in a pneumatic lip seal. *Tribol Int* 1999; 32(1):113.
- [2] Pinedo B, Aguirrebeitia J, Conte M, Igartua A. Tri-dimensional eccentricity model of a rod lip seal. *Tribol Int* 2014; 78:6874.
- [3] Lee CY, Lin CS, Jian RQ, Wen CY. Simulation and experimentation of the contact width and pressure distribution of lip seals. *Tribol Int* 2006;39(9):91520.
- [4] Belforte G, Conte M, Manuello A, Mazza L, Visconte C. Experimental and numerical evaluation of contact pressure in pneumatic seals. *Tribol Int* 2009;42(1):169-75
- [5] Belforte G, Conte M, Mazza L, Raparelli T, Visconte C. Test rig for rod seals contact pressure measurement. *WIT Transactions on Engineering Sciences*. 66. Southampton and Boston: WIT Press; 2010. p. 10714.
- [6] M. E. Van Valkenburg, *Analog Filter Design*, Holt, Rinehart & Winston, 1982
- [7] Fern A, Jones AM, Pham DT, Wang J. Finite element analysis of a valve stem seal, SAE Paper 980580, 1998.
- [8] MSC Marc 2001. User manual.

